e-HIGHWAY 2050

Modular Development Plan of the Pan-European Transmission System 2050

Contract number	308908	**Instrument**	Collaborative Project
Start date	1st of September 2012	**Duration**	40 months
WP 8	**Enhanced Pan-European Transmission Planning Methodology**		
D 8.5.a	Enhanced methodology to assess robustness of a grid architecture		

		Date & Visa
Written by	Francisco Echavarren, Luis Rouco, Lukas Sigrist, COMILLAS	18/06/2015
Checked by	Peter Van Roy, ELIA Alexander Weber, TU BERLIN Patrick Panciatici, Jean Maeght, Camille Pache, RTE	24/06/2015
Validated by	Gérald Sanchis, Nathalie Grisey, RTE	14/09/2015

Project co-funded by the European Commission within the Seventh Framework Program		
Dissemination Level		
PU	Public	X
PP	Restricted to other program participants (including the Commission Services)	
RE	Restricted to a group specified by the consortium (including the Commission Services)	
CO	Confidential, only for members of the consortium (including the Commission Services)	

Document information

General purpose

This document is the deliverable D8.5.a of the e-Highway2050 project. It contains the description of the work performed in the framework of Task 8.5, named *"Enhanced methodology to assess robustness of a grid architecture"*.

Change status

Revision	Date	Changes description	Authors
V0.0	26/03/2015	Initial version	F. Echavarren L. Rouco L. Sigrist
V1.0	22/05/2015	Modifications after exchanges within WP8	L. Rouco
V1.1	18/06/2015	Modifications after review by the quality pool	C. Pache
V1.2	03/09/2015	Modifications after review by project partners	F. Echavarren L. Sigrist

EXECUTIVE SUMMARY

Task WP8.5 is aimed at investigating the robustness of the grid architectures proposed by previous tasks of Work Package WP8. This report proposes sanity checks which verify if a grid architecture can be operated without major voltage and stability issues. The proposed robustness analysis should also give warnings to the planner and help anticipate deep changes in the power system.

The robustness analysis involves the study of voltage-reactive power control and stability, transient stability and small-signal stability.

Voltage-reactive control and stability is concerned with the ability of the power system to supply its loads at admissible voltages. Voltage control analysis is aimed at determining reactive power resources to ensure that voltage profile is within admissible ranges. Voltage stability analysis computes the load margin to voltage collapse. Voltage-reactive power control and stability is addressed using steady-state models and AC load flow tools.

Transient stability is interested in the ability of synchronous generators to remain in synchronism in case of faults that may occur. Transient stability of a power system is measured by the critical clearing times of the faults. Critical clearing times below times of protections might either affect the design of the grid or require special protection schemes (defence plans).

Small-signal stability looks at the damping of the electromechanical oscillations of synchronous generators. Should the damping of electromechanical oscillations be below a safe value, power system stabilizer of generators must be redesigned. Damping controllers of FACTS devices and HVDC links can also contribute to the damping of generator oscillations.

An AC load flow model of the grid is needed to account for reactive power flows and bus voltage magnitude variation. As the previous tasks of this work package (WP8) have been using DC load flow models, an AC load flow model will be built from the DC load flow one (which is the input of the task). The construction of the AC load flow model involves the dispatch of voltage-reactive power control resources (shunt devices, transformer taps, generator setpoint voltages). Moreover, the possibility of AC load flow lack of convergence has also been addressed.

Transient and small-signal stability analyses not only need the steady-state model of the network provided by an AC load flow, but also the dynamic model of generators and other dynamic devices. Simplified models of synchronous generators have been used instead of detailed models whenever those models are not available. In addition to synchronous generators models, wind generator and HVDC links might have to be added. Hence, it has to be investigated if simplified models of wind generators and HVDC links can be used.

At the time of completing this report, tests cases produced by previous tasks of this work package were not available yet. Thus, the proposed approach has been tested on large scale models of the Spanish and French power systems. It will be tested on a larger European test case in task 8.6. Small-signal stability analysis will also be presented in the next deliverable D8.6 “Detailed enhanced methodology for long-term grid planning and specification of tools

associated with the enhanced methodology", as it was still under progress at the time of writing.

The following conclusions have been drawn from the work carried out so far:

- A procedure to build an AC load flow model from the DC load flow one has been developed. The procedure dispatches voltage-reactive power control resources to attain AC load flow within an admissible voltage range. However, the main issue of this method was the convergence of the initial load flow which could occur in a planning study and does not occur on actual realized data. If the initial AC load flow does not converge, a new algorithm has been proposed and implemented. It is based on a non-divergent load flow and a sensitivity based algorithm. If a divergent load flow problem occurs, a sequential combination of a non-divergent load flow algorithm and a sensitivity algorithm is used. The performance of the procedure has been tested on actual scenarios of the Spanish and French power systems. The results are very promising.

- The flexibility and robustness of the algorithm to assess voltage stability of large power systems has been shown. The maximum load that generators can serve (or the maximum loadability of the power system) has been determined. The voltage stability of a power system has been measured using the distance to the point to maximum loadability of the power system or point of voltage collapse.

- An investigation on the impact of models and controls of wind generators and HVDC links on the transient stability has been carried out. It has found that simplified models of power system components should be avoided. Moreover, it has been found that some controls contribute to improve the transient stability of the power system, whereas other controls deteriorate it. Therefore, robustness of grid architectures would rely on appropriate control schemes. Part of the results of this investigation have been summarized in the paper "A fundamental study on the impact of HVDC lines on transient stability of power systems" by L. Sigrist, F. Echavarren, L. Rouco and P. Panciatici that has been accepted for presentation at the IEEE Power Tech 2015.

- Preliminary results of the procedure to build a dynamic model and to assess transient stability have been shown. Meaningful results have been obtained: the critical clearing times are within the typical range.

The developed prototypes to address robustness analysis are described in deliverable D8.5.b "Prototype to assess robustness of a grid architecture".

TABLE OF CONTENTS

Acronyms and definitions

AC/DC	Alternate/Direct Current
HVDC	High Voltage Direct Current
LCC	Line Commutated Converter
VSC	Voltage Source Converter
DFIG	Doubly Fed Induction Generator
MSG	Multipole Synchronous Generator
TSO	Transmission System Operator
PSS/E	Power System Simulator

Notation

$\boldsymbol{\theta}$	Vector of bus voltage angles
$\mathbf{V}$	Vector of bus voltage magnitudes
$\mathbf{P}_{\boldsymbol{G}}$	Vector of bus active power generations
$\mathbf{P}_{\boldsymbol{D}}$	Vector of bus active power demands
$\mathbf{B}'$	Susceptance matrix of DC power flow model
$\boldsymbol{P_{ij}}$	Active power through branch from i-th bus to j-the bus
$\boldsymbol{x_{ij}}$	Reactance of branch from i-th bus to j-the bus
$\boldsymbol{r_{ij}}$	Resistance of branch from i-th bus to j-the bus
$\mathbf{P}_{\boldsymbol{Lij}}$	Active power losses in branch from i-th bus to j-the bus
$\mathbf{P}_{\boldsymbol{D}}$	Vector of bus active power losses due to branch losses
$\boldsymbol{b_{ij}}$	Susceptance of branch from i-th bus to j-the bus
$\mathbf{x}$	Vector of state variables of AC power flow equations
$\mathbf{g}$	Vector of non-linear functions of AC power flow equations
$\mathbf{P}$	Vector of bus active power equations of AC power flow equations
$\mathbf{Q}$	Vector of bus reactive power equations of AC power flow equations
$\mathbf{J}$	Jacobian matrix AC power flow equations
$\boldsymbol{\Delta}\mathbf{P}$	Bus active power mismatches
$\boldsymbol{\Delta}\mathbf{Q}$	Bus reactive power mismatches
$\mathbf{gC}$	Vector of critical set of non-linear functions of power flow equations
$\mathbf{u}$	Vector of control actions of AC power flow solutions
$\boldsymbol{Q_{gi}^{max}}$	Maximum reactive power generation capability of i-the generator

List of Figures

List of Tables

1. Introduction

Task 8.5 is aimed at investigating the robustness of the grid architectures proposed by previous tasks of Work Package WP8 (tasks from 8.1 through 8.4). This report proposes sanity checks which verify if a grid architecture can be operated without major voltage and stability issues. The proposed robustness analysis should also give warnings to the planner and help anticipate deep changes in the power system.

The robustness analysis involves the study of voltage-reactive power control and stability, i.e. transient stability and small-signal stability.

Voltage-reactive control and stability is concerned with the ability of the power system to supply its loads at admissible voltages. Voltage control analysis is aimed at determining reactive power resources to ensure that voltage profile is within admissible ranges. Voltage stability analysis computes the load margin to voltage collapse. Voltage-reactive power control and stability is addressed using steady-state models and AC load flow tools.

Transient stability is interested in the ability of synchronous generators to remain in synchronism in case of faults that may occur. Transient stability of a power system is measured by the critical clearing times of the faults. Critical clearing times below times of protections might either affect the design of the grid or require special protection schemes (defence plans).

Small-signal stability looks at the damping of the electromechanical oscillations of synchronous generators. Should the damping of electromechanical oscillations be below a safe value, power system stabilizer of generators must be redesigned. Damping controllers of FACTS devices and HVDC links can also contribute to the damping of generator oscillations.

An AC load flow model of the grid is needed to account for reactive power flows and bus voltage magnitude variation. As the previous tasks of this work package (WP8) have been using DC load flow models, an AC load flow model will be built from the DC load flow one (which is the input of the task). The construction of the AC load flow model will involve the dispatch of voltage-reactive power control resources (shunt devices, transformer taps, generator setpoint voltages). Moreover, the possibility of AC load flow lack of convergence will be also addressed.

Transient and small-signal stability analyses not only need the steady-state model of the network provided by an AC load flow, but also the dynamic model of generators and other dynamic devices. Simplified models of synchronous generators have been used instead of detailed models whenever those models are not available. In addition to synchronous generators models, wind generator and HVDC links might have to be added. Hence, it has to be investigated if simplified models of wind generators and HVDC links can be used.

The report contains a chapter devoted to each step of our approach to test the robustness of the proposed grid architectures conducted so far:

- Development of an AC load flow model from a DC one
- Voltage stability analysis
- Impact of models and controls of wind generators and HVDC links on system dynamic performance
- Transient stability analysis

The proposed approach will be tested firstly on large scale models of the Spanish and French power systems.

At the time of completing this report, tests cases produced by previous tasks of this work package are not available yet. Small-signal stability analysis is under progress as well.

2. Development of an AC load flow model from a DC one

An AC load flow model of the grid is needed to account for reactive power flows and bus voltage magnitude variation. As the previous tasks of this work package (WP8) have been using DC load flow models, an AC load flow model will be built from the DC load flow one. The construction of the AC load flow model will involve the dispatch of voltage-reactive power control resources (shunt devices, transformer taps, generator setpoint voltages). Moreover, the possibility of AC load flow lack of convergence will be addressed.

2.1. Procedure

A procedure to build a fully detailed AC load flow from its DC approximation model data has been developed. Figure 2-1 shows the flowchart of the developed procedure.

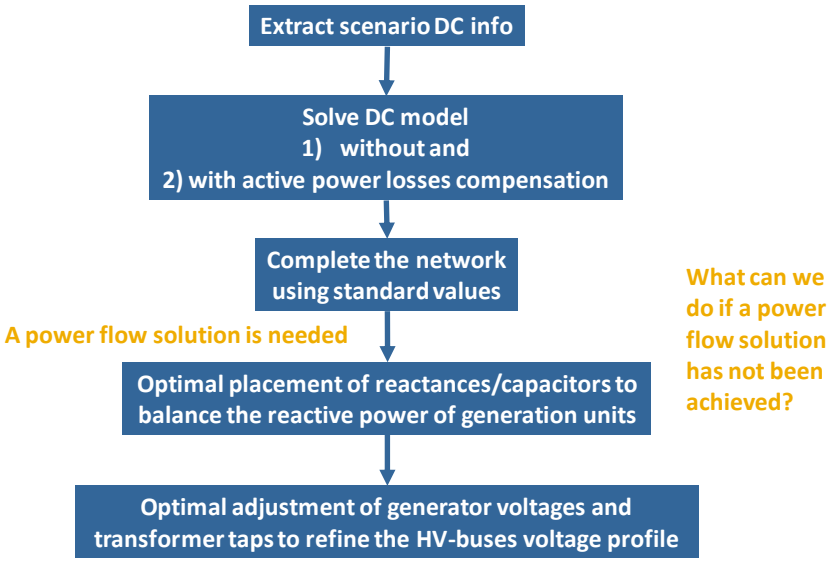

Figure 2-1. Procedure to build an AC load flow model from a DC one

The DC load flow model does not account for (active power) losses. Hence, losses must be estimated to incorporate generation to supply losses in order to avoid that losses are only supplied by the swing bus in the AC load flow solution. If losses were to be supplied by the swing bus, power flow of branches close to the swing bus might be distorted [1].

The DC load flow equations are:

$$\mathbf{B}'\boldsymbol{\theta} = \mathbf{P}_G - \mathbf{P}_D$$

Once bus voltage angles $\boldsymbol{\theta}$ have been determined, branch power flows are computed as follows:

$$P_{ij} = \frac{\theta_i - \theta_i}{x_{ij}}$$

$$P_{Lij} = r_{ij} P_{ij}^2$$

Then, the generation dispatch is updated to supply those losses.

The DC load flow equations are updated incorporating branch losses according to:

$$\mathbf{B'\theta} = \mathbf{P}_G - \mathbf{P}_D - \mathbf{P}_L$$

The updated solution of the DC load flow equations provides an initial guess of the bus voltage angles to be used in the solution of the AC load flow.

The branch data in the DC load flow data set contains branch resistance and reactance. Transmission line data includes line length. The total line susceptance is computed using pu/length susceptance using data of standard overhead lines contained in Table 2.I. The line length is determined from the actual line reactance and the pu/length reactance of a standard overhead line (the parameters of typical 400 and 220 kV lines have been taken from the Spanish Operational Procedure (Grid Code) 13.1 that provides the criteria for the development of the transmission grid [2]).

Table 2.I. Parameters of standard overhead transmission lines (pu of 100 MVA)

Voltage	Conductor	Maximum current (A)	R (pu/100 km)	X (pu/100 km)	B (pu/100 km)
400 kV	Condor triplex	2500	0.00161	0.01729	0.66554
220 kV	Gull duplex	2000	0.00956	0.06518	0.17790

The computation of the AC load flow solution also requires reactive power consumption of the loads (load power factor) and reactive power capability (both maximum generation and consumption capability) of generators. Although load power factor and generator reactive power capability are parameters that can be set by the user, we have assumed:

- Load power factor: 0.989 (it means that QL=0.15*PL)
- Generator reactive power capability: maximum generation PF = 0.9 lagging (QGMAX=PGMAX*tan(acos(0.9)), minimum generation PF = 0.95 leading (QGMIN=-PGMAX*tan(acos(0.95)),

These parameters have been taken from Spanish Operational Procedure (Grid Code) 7.4 that organizes the provision of the voltage control ancillary service [3]. These parameters can be chosen freely by the user.

AC load flow is first solved using a flat voltage magnitude starting point (1 pu). The voltage profile must be tuned by:

- Placement of shunt reactors/capacitors
- Adjustment of transformer taps and scheduled generator voltages

Placement of reactors/capacitors is done:

- Assuming an initial power flow solution without reactive limits on generators, place reactors/capacitors to reduce reactive power violations of generation units

$$\mathbf{J}\begin{bmatrix}\mathbf{\Delta\theta}\\ \mathbf{\Delta V}\\ \hline \mathbf{V}\end{bmatrix} = \begin{bmatrix}\mathbf{\Delta P}\\ \mathbf{\Delta Q}\end{bmatrix}$$

$$\min \sum_i \left(Q_{Gi} - Q_{Gi}^0\right)$$

- Use first order sensitivities to identify most efficient buses

$$\frac{\mathrm{d}\mathbf{Q}_G}{\mathrm{d}\mathbf{Q}} = \frac{\partial \mathbf{Q}_G}{\partial \mathbf{x}}\left(\frac{\partial \mathbf{g}}{\partial \mathbf{x}}\right)^{-1}\frac{\partial \mathbf{g}}{\partial \mathbf{Q}}$$

- The stopping criteria is when the maximum of reactive power to be installed is reached

The maximum reactive power compensation to be installed can be chosen freely by the user. A meaningful value can be estimated from the system reactive power requirements that cannot be supplied by generators derived from the DC load flow solution.

$$\mathbf{Q}_C = \sum_b x_b P_b^2 + \sum_l Q_{Dl} - \sum_\ell b_\ell - \sum_g Q_{Gg}^{max}$$

where:

$\sum_b x_b P_b^2$ is the total reactive power consumed by branches (transmission lines and transformers)
$\sum_l Q_{Dl}$ is the total reactive power demanded by the loads
$\sum_\ell b_\ell$ is the total reactive power produced by transmission lines
$\sum_g Q_{Gg}^{max}$ is the total reactive power generation capability of generators

Adjustment of generator voltages and transformer taps is done:

- Identifying unsolved reactive power violations and most efficient control actions
- Using first order sensitivities to identify most efficient devices
- The stopping criteria is when the improvement between iterations is below a minimum level

The performance of the procedure has been tested on actual scenarios of the Spanish power system and of the French power system (AC-to-DC-to-AC). As these initial scenarios are actual AC test cases, DC approximation models are first constructed from the original AC scenarios. Then, the developed method is applied to rebuild the AC models from the DC approximation and compare them to the original AC scenarios. The results are very satisfactory.

However, the main issue of this method was the convergence of the initial load flow. In a planning study, divergence of the load flow calculation is likely to occur, contrary to the test cases based on actual realized data. If the initial AC load flow does not converge, a new algorithm has been proposed and implemented. Figure 2-2 shows the flowchart of developed algorithm.

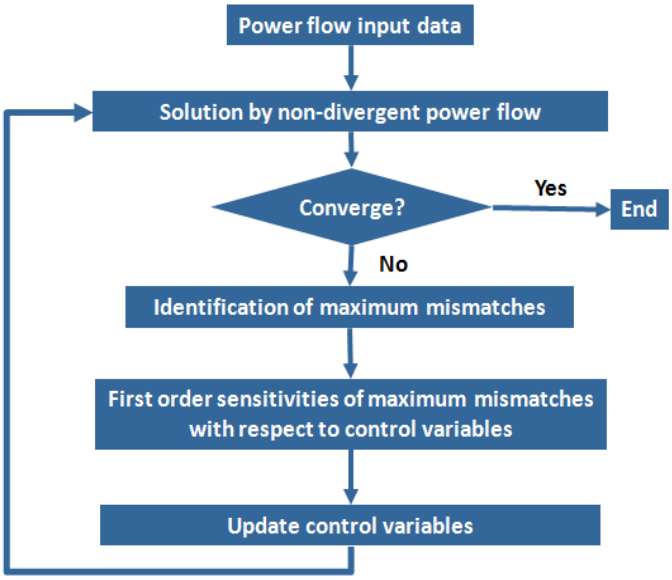

Figure 2-2. Algorithm to address AC load flow lack of converge

If a divergent load flow problem occurs, a sequential combination of a non-divergent load flow algorithm and a sensitivity algorithm is used.

A non-divergent power flow updates the state variables $\mathbf{x}$ according to

$$\mathbf{x}^{k+1} = \mathbf{x}^k + d \cdot \Delta\mathbf{x}^k$$
$$\Delta\mathbf{x}^k = \left(-\left(\frac{\partial \mathbf{g}}{\partial \mathbf{x}}\right)^{-1} \right)^k \cdot \mathbf{g}^{\mathbf{k}}$$

where d is a step-control parameter that allows to only make small changes to the state variables in every step, and:

$$\mathbf{x} = [\boldsymbol{\theta}^{\mathrm{T}} \quad \mathbf{V}^{\mathrm{T}}]^{\mathrm{T}}$$
$$\mathbf{g} = \begin{bmatrix} \mathbf{P}(\boldsymbol{\theta}, \mathbf{V}) \\ \mathbf{Q}(\boldsymbol{\theta}, \mathbf{V}) \end{bmatrix}$$

If any value of the step-control parameter d cannot improve the mismatches, the power flow is considered unsolvable and $\mathbf{x}^k$ corresponds with the maximum mismatches point.

The sensitivities of the most critical mismatches set ($\mathbf{gC}$) with respect to control actions $\mathbf{u}$ (shunt devices or Q load) are computed and used to determine the most efficient control actions as:

$$\frac{\mathrm{d}\mathbf{gC}}{\mathrm{d}\mathbf{u}} = \frac{\partial \mathbf{gC}}{\partial \mathbf{u}} - \frac{\partial \mathbf{gC}}{\partial \mathbf{x}} \left(\frac{\partial \mathbf{g}}{\partial \mathbf{x}}\right)^{-1} \left(\frac{\partial \mathbf{g}}{\partial \mathbf{u}}\right)$$

2.2. Illustrative examples

Large scale models of the Spanish and the French power systems have been used to test the proposed algorithms. Table 2.II provides the features of them. The total number of buses, generators, lines and transformers are provided. Both systems have similar sizes.

Table 2.II. Features of the test cases

	Spanish Power System	French Power System
Number of buses	1838	1823
Number of buses 400 kV	219	517
Number of buses 220 kV	623	1258
Number of buses < 220 kV	996	48
Number of generators	742	314
Number of lines	2084	2283
Number of lines 400 kV	362	700
Number of lines 220 kV	842	1577
Number of lines < 220 kV	880	6
Number of transformers	723	413

2.2.1. Spanish power system

Table 2.III provides a summary of the operating point (summer peak load 2012 that took place at 14:00 of 28 June 2012) of the Spanish power system used as starting point. Active power losses are around 2% of active power generation. There is a surplus of reactive power that must be absorbed by generators. Figure 2-4 shows the cumulative distribution of bus voltages. It confirms that the voltage profile is above the nominal voltage and that the voltage profile of 220 kV is below the voltage profile of 400 kV.

Table 2.III. Summary of the operating point of the Spanish power system

	GEN	SHUNT	LINES	DEMAND	LOSSES
P [MW]	41469.6	0.0	0.0	40612.2	857.4
Q [MVAr]	-658.6	-5330.3	22695.4	6237	10469.6

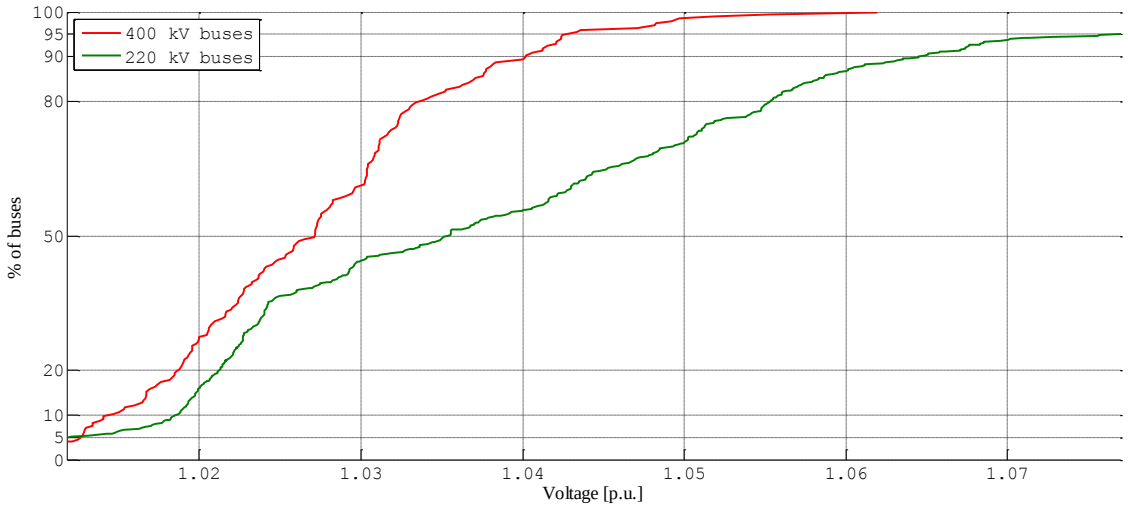

Figure 2-3. Spanish power system: cumulative distribution of bus voltages

Although load power factor is a parameter that can be chosen by the user, we have assumed that it is 0.989 lagging (QL=0.15PL) which is actually the value required by the Spanish TSO to DSOs. Figure 2-4 shows the cumulative distribution of the load power factor. It confirms that the selected value of the load power factor reflects the actual behaviour of the system.

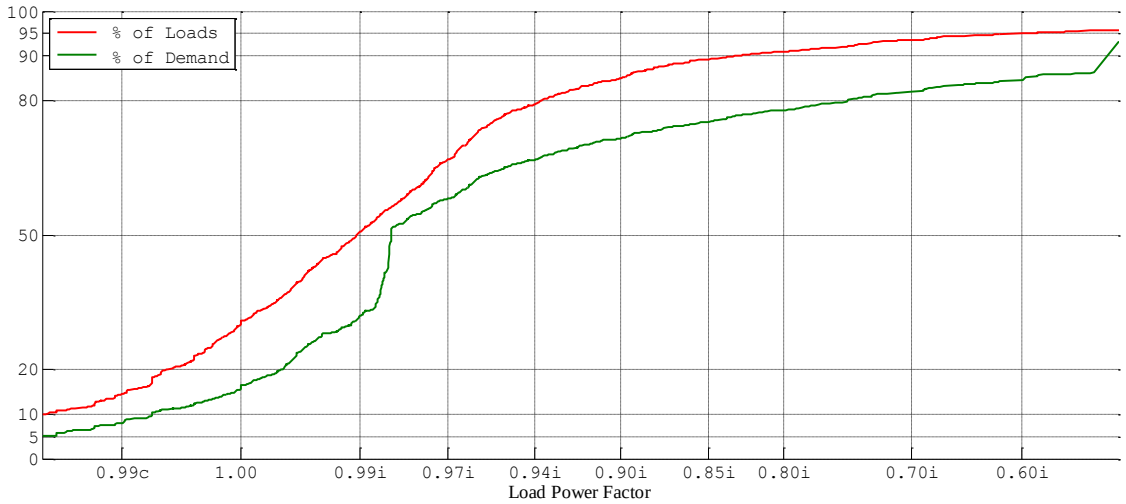

Figure 2-4. Spanish power system: cumulative distribution of load power factor

No load flow convergence issues

The performance of the algorithm to tune the AC load flow solution is firstly illustrated comparing the original shunt devices and the proposed shunt devices.
shows that reactors and capacitors proposed in each area of the Spanish system are very close to the actual reactors and capacitors connected.

Table 2.IV. Spanish power system: Performance of the algorithm to tune AC load flow solution: original shunt devices and proposed shunt devices

	CAPACITORS		REACTORS	
AREA	original	estimated	original	estimated
NOROESTE	64	50	-710	-800
NORTE	0	0	-998	-850
ESTE	242	250	-675	-550
CENTRO	273	350	-1857	-1750
SUR	0	0	-1380	-1200
TOTAL	**579**	**650**	**-5620**	**-5150**

Moreover, the quality of the AC load flow solution is measured comparing the cumulative distribution of mismatches in line power flows and bus voltages between the original AC data and the reconstructed AC results.

Figure 2-5 and Figure 2-6 compare respectively the cumulative distribution of errors of 400 and 220 kV power flows. Power flows obtained from DC approximation, DC approximation including losses, AC load flow solution with flat start and AC load flow solution after voltage control actions are compared with the actual power flows. Successive refinements achieve reduction of errors.

Figure 2-7 and Figure 2-8 compare respectively the cumulative distribution of 400 and 220 kV bus voltages errors.

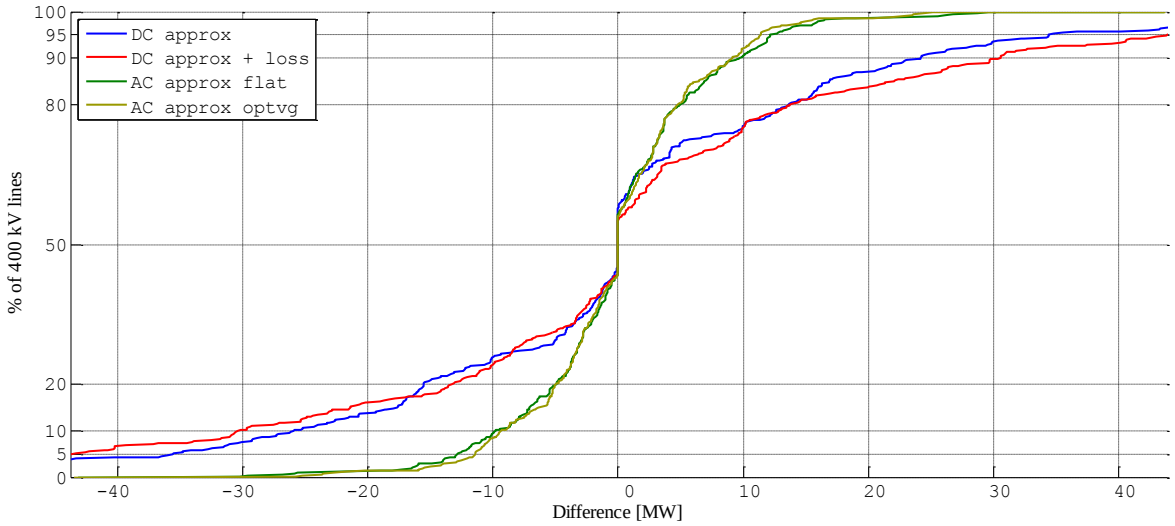

Figure 2-5. Spanish power system: cumulative distribution of mismatches in 400 kV line power flows

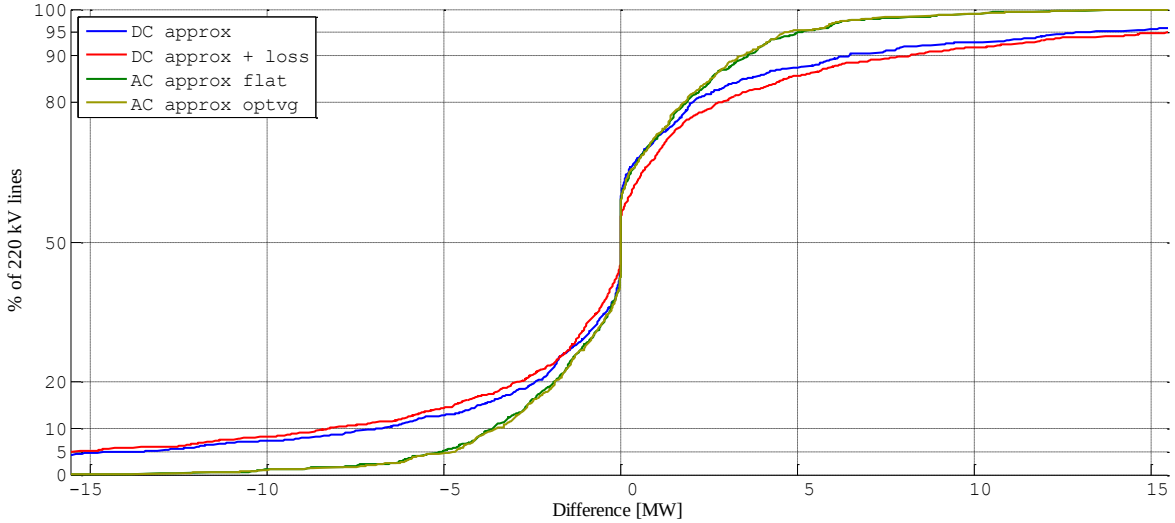

Figure 2-6. Spanish power system: cumulative distribution of mismatches in 220 kV line power flows

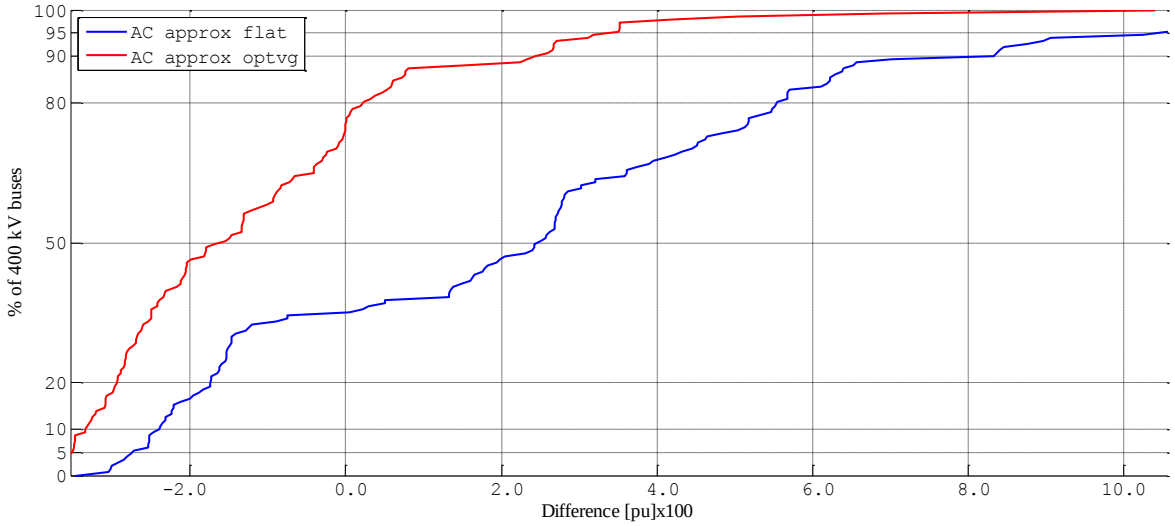

Figure 2-7. Spanish power system: cumulative distribution of mismatches in 400 kV bus voltages

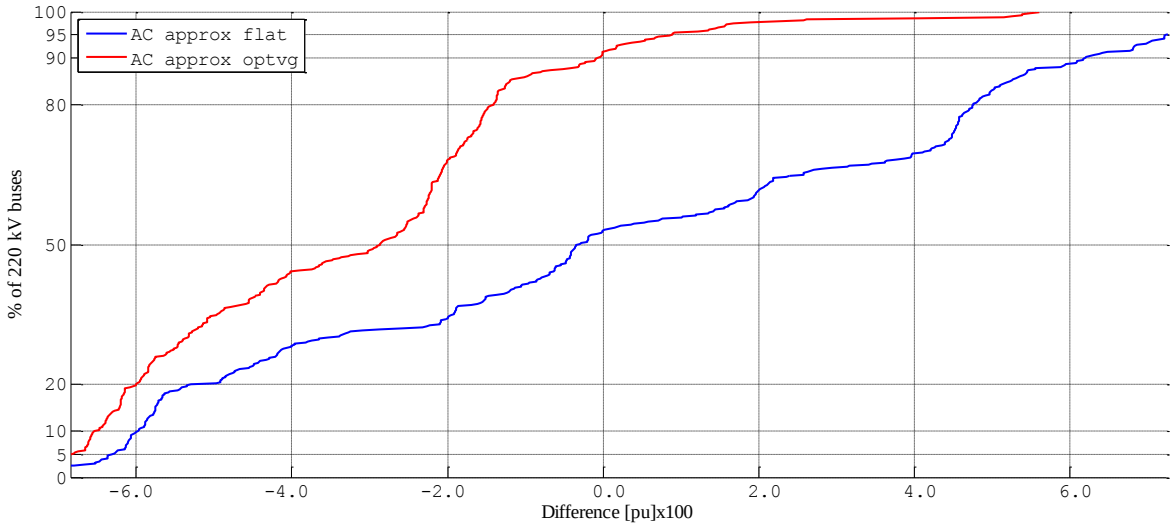

Figure 2-8. Spanish power system: cumulative distribution of mismatches in 220 kV bus voltages

Load flow convergence issues

The model of the Spanish power system that we have considered does not exhibit AC load flow lack of convergence. However, we could push the system against its limits changing the power factor of the loads in order to be able to test the methodology. We have considered two alternatives to deal with AC load flow lack of convergence: shunt devices control and reactive load control.

Table 2.V illustrates the performance of the algorithm to address AC load flow lack of convergence by shunt devices control requirements as a function of load power factor. If the load power factor is equal or lower than 0.7 the AC load flow does not initially converge. AC load flow lack of convergence has been solved connecting shunt devices (capacitors).

Table 2.VI illustrates the performance of the algorithm to address AC load flow lack of convergence by reactive load control requirements as a function of load power factor. AC load flow lack of convergence has been solved by disconnecting reactive power load.

It should be noted that the AC load flow exhibits convergence problems only in case of 0.7 power factor loads.

Acting upon the load continuously becomes more effective than connecting discrete shunt devices.

Table 2.V. Spanish power system: Performance of the algorithm to address AC load flow lack of convergence: shunt devices control requirements as a function of load power factor

By shunt device control						
Load PF	0.989	0.9	0.85	0.8	0.75	0.7
QL [MVAr]	7660	24805	31741	38279	45168	52251
B [MVAr]	0	0	0	0	0	1927

Table 2.VI. Spanish power system: Performance of the algorithm to address AC load flow lack of convergence: reactive load control requirements as a function of load power factor

By reactive load control						
Load PF	0.989	0.9	0.85	0.8	0.75	0.7
QLinitial [MVAr]	7660	24805	31741	38279	45168	52251
QLfinal [MVAr]	7660	24805	31741	38279	45168	52051
DeltaQL [MVAr]	0	0	0	0	0	-200

2.2.2. French power system

Table 2.VII provides a summary of the operating point (winter peak load 2012 that took place at 19:10 of 6 February 2012) of the French power system used as starting point. Active power losses are around 2% of active power generation. There is a deficit of reactive power that must be supplied by generators. Figure 2-4 shows the cumulative distribution of bus voltages. It confirms that thanks to generator reactive power generation, the voltage profile is above the nominal voltage. In contrast to the Spanish power system, the voltage profile of 220 kV is above the voltage profile of 400 kV.

Table 2.VII. Summary of the operating point of the French power system

	GEN	SHUNT	LINES	DEMAND	LOSSES
P [MW]	104323.1	0.0	0.0	102134.0	2189.1
Q [MVAr]	15909.6	1938.0	30692.2	21493.8	27046.0

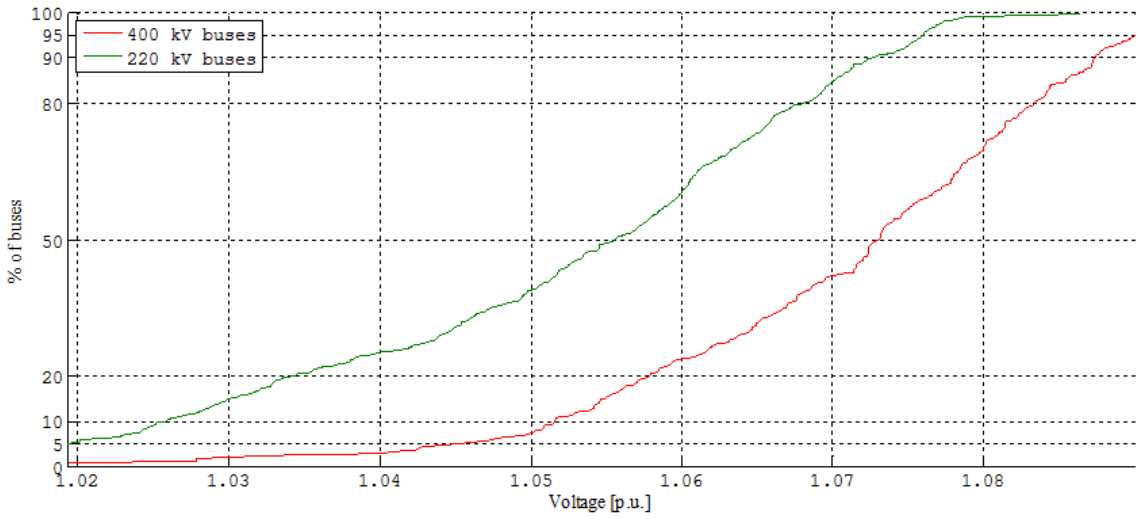

Figure 2-9: French power system: cumulative distribution of bus voltages

The actual load power factor is also investigated in case of the French power system. Figure 2-10 shows the cumulative distribution of the load power factor. It confirms that the selected value of the load power factor (it has 0.989 lagging which means that QL=0.15PL) reflects the actual behaviour of the system.

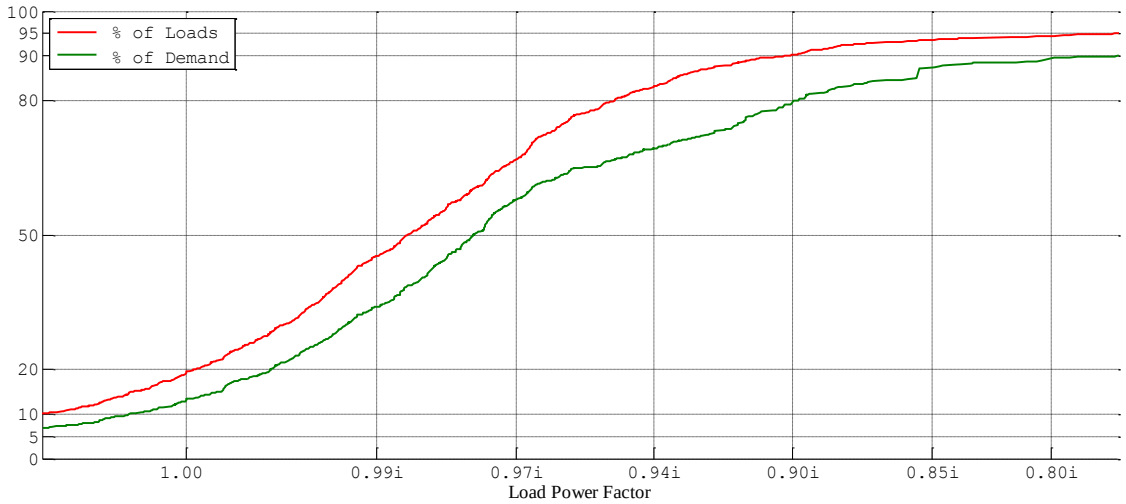

Figure 2-10: French power system: cumulative distribution of load power factor

No load flow convergence issues

The performance of the algorithm to tune the AC load flow solution is firstly illustrated comparing the original shunt devices and the proposed shunt devices. Table 2.VIII shows that reactors and capacitors proposed in each area of the French system are very close to the actual reactors and capacitors connected.

Table 2.VIII. French power system: Performance of the algorithm to tune AC load flow solution: original shunt devices and proposed shunt devices

	CAPACITORS		REACTORS	
AREA	original	estimated	original	estimated
AREA 01	0	0	400	750
AREA 02	0	0	0	0
AREA 03	0	-50	0	0
AREA 04	0	0	240	0
AREA 05	0	-100	480	450
AREA 07	0	0	640	350
AREA 08	0	0	78	250
AREA AT	0	0	0	0
AREA BE	0	0	0	0
AREA CH	0	0	0	0
AREA DE	0	0	0	0
AREA ES	-128	0	0	0
AREA GB	0	0	0	0
AREA IT	0	0	0	0
AREA NL	0	0	0	0
TOTAL	**-128**	**-150**	**1838**	**1800**

Moreover, the quality of the AC load flow solution is measured comparing the cumulative distribution of mismatches in line power flows and bus voltages.

Figure 2-11 and Figure 2-12 compare respectively the cumulative distribution of errors of 400 and 220 kV power flows. Power flows obtained from, AC load flow solution with flat start, AC load flow solution after shunt reactors and capacitors connection and AC load flow with generator voltage control actions are compared with the actual power flows. Successive refinements achieve reduction of errors.

Figure 2-13 and Figure 2-14 compare respectively the cumulative distribution of mismatches in 400 and 220 kV bus voltages. Bus voltages obtained from, AC load flow solution with flat start, AC load flow solution after shunt reactors and capacitors connection and AC load flow with generator voltage control actions are compared with the actual bus voltages. Successive refinements achieve reduction of errors.

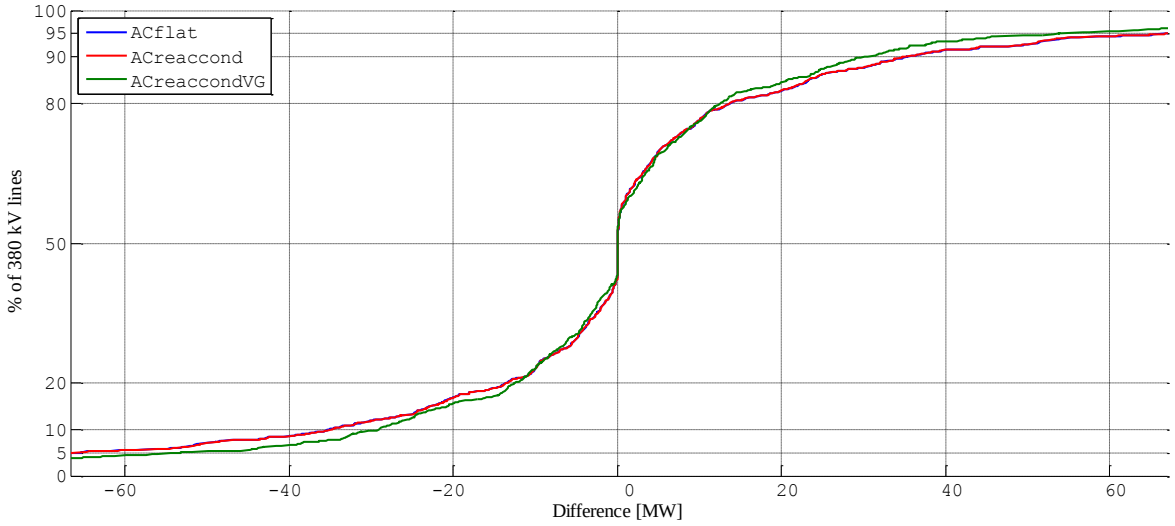

Figure 2-11: French power system: cumulative distribution of mismatches in 400 kV line power flow errors

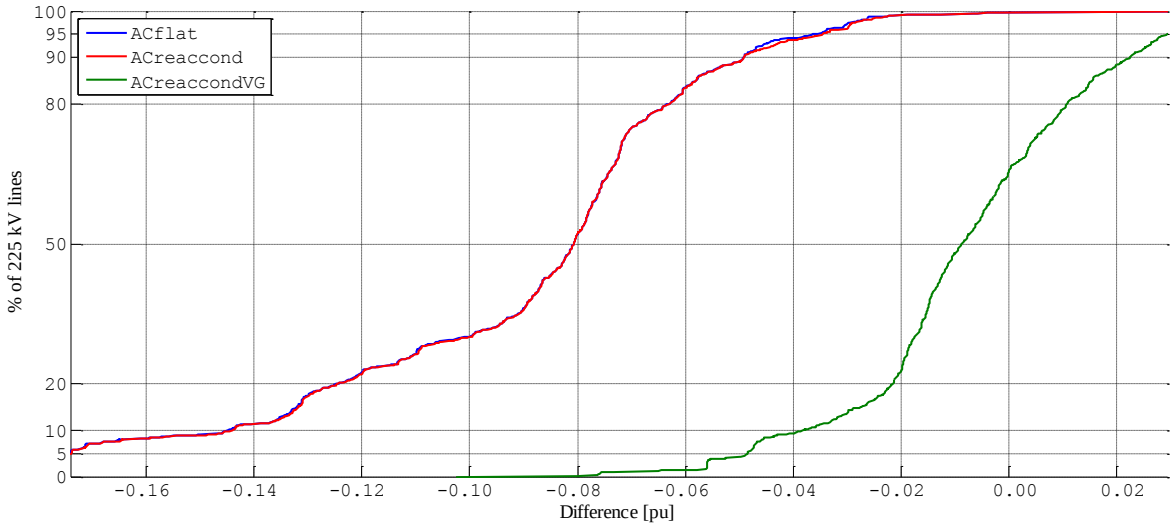

Figure 2-12: French power system: cumulative distribution of mismatches in 220 kV line power flows errors

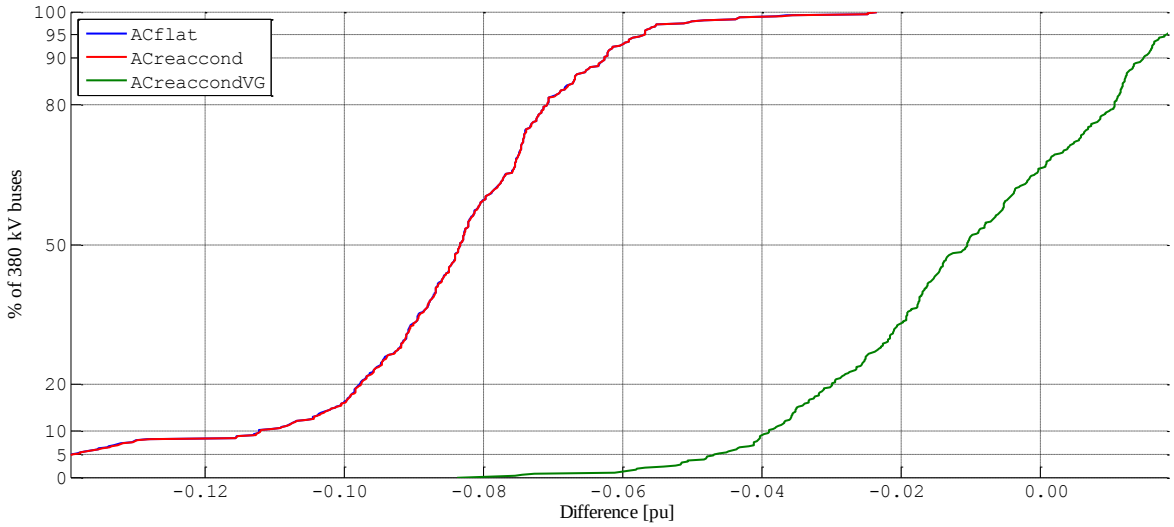

Figure 2-13: French power system: cumulative distribution of mismatches in 400 kV bus voltage errors

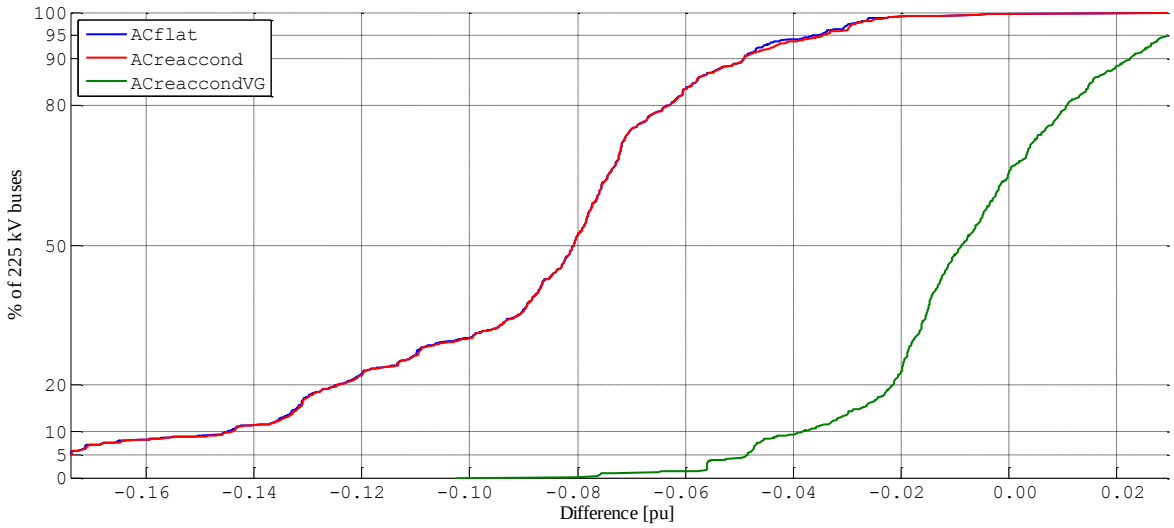

Figure 2-14: French power system: cumulative distribution of mismatches in 220 kV bus voltage errors

Load flow convergence issues

The model of the French power system that we have considered does not exhibit AC load flow lack of convergence. However, we could push the system against its limits by changing the power factor of the loads. We have considered two alternatives to deal with AC load flow lack of convergence: shunt devices control and reactive load control.

illustrates the performance of the algorithm to address AC load flow lack of convergence by shunt devices control requirements as a function of load power factor. If the load power factor is equal or lower than 0.9 the AC load flow does not initially converge. AC load flow lack of convergence has been solved connecting shunt devices (capacitors).

Table 2.X illustrates the performance of the algorithm to address AC load flow lack of convergence by reactive load control requirements as a function of load power factor. AC load flow lack of convergence has been solved disconnecting reactive power load.

It should be noted that the AC load flow does exhibit convergence problems in case of 0.9 (or lower) power factor loads, which is faster than the Spanish test case (0.7).

Acting upon the load continuously becomes more effective than connecting discrete shunt devices.

Table 2.IX. French power system: Performance of the algorithm to address AC load flow lack of convergence: shunt devices control requirements as a function of load power factor

By shunt device control						
Load PF	0.989	0.980	0.950	0.900	0.850	0.801
QL [MVAr]	17420	23651	38282	56410	72183	87050
B [MVAr]	0	0	0	300	2052	11641

Table 2.X. Spanish power system: Performance of the algorithm to address AC load flow lack of convergence: shunt devices or reactive load control requirements as a function of load power factor

By reactive load control						
Load PF	0.989	0.980	0.950	0.900	0.850	0.801
QLinitial [MVAr]	17420	23651	38282	56410	72183	87050
QLfinal [MVAr]	17420	23651	38282	56277	71368	80448
DeltaQL [MVAr]	0	0	0	-133	-815	-6602

2.3. Partial conclusions

A procedure to build an AC load flow model from the DC load flow one has been developed. The procedure dispatches voltage-reactive power control resources to attain AC load flow within an admissible voltage range. Connection of shunt devices (reactors and capacitors) is determined firstly. Transformer taps and generator voltages are tuned subsequently. Voltage-reactive power control resources are managed using first order sensitivities.

However, the main issue of this method was the convergence of the initial load flow which could occur in a planning study and does not occur on actual realized data. If the initial AC load flow does not converge, a new algorithm has been proposed and implemented. It is based on a non-divergent load flow and a sensitivity based algorithm. If a divergent load flow problem occurs, a sequential combination of a non-divergent load flow algorithm and a sensitivity algorithm is used.

The performance of the procedure has been tested on actual scenarios of the Spanish and French power systems. The results are very promising.

3. Voltage stability analysis

Voltage stability is concerned with the ability of the system to supply its loads at acceptable voltage levels. Voltage stability analysis computes the load margin to voltage collapse as a measure of the voltage security margin.

3.1. Study method

Voltage stability is becoming one of the most important issues in the power systems due to the intensive use of the transmission networks. Voltage stability is concerned with the ability of a power system to maintain acceptable bus voltages under normal conditions and after being subjected to a disturbance [4]. The accurate representation of the voltage instability phenomena requires a detailed model of power system components (generators, transformers, loads, etc.). The risk of voltage instability of a power system can be measured by the distance of the steady-state power flow equations from the initial point of operation (base case) to its saddle node bifurcation point, known as the voltage collapse point. This distance is usually called stability margin [16]. Given a set of power flow equations $\mathbf{g}(\mathbf{x}, \lambda) = \mathbf{0}$ where x represents the state variables, i.e. bus voltages magnitude and angle, and λ a power dispatch parameterization factor. Therefore the voltage collapse point will correspond to the solution of the optimization problem ([17], [18]):

$$\begin{aligned} &\max\ \lambda \\ &s.t.\ \ \mathbf{g}(\mathbf{x}, \lambda) = \mathbf{0} \end{aligned}$$

The solution of the optimization problem not only satisfies power flow equations $\mathbf{g}(\mathbf{x}, \lambda) = \mathbf{0}$, but also implies the singularity of the jacobian $\mathbf{g_x} = \partial \mathbf{g} / \partial \mathbf{x}$.

From a physical point of view, the stability margin of a power system can be affected by a number of features of the power network, such as the generator voltages, the load of the system, or the generation–demand imbalance between the power system areas. One important fact when analyzing voltage collapse phenomena is that the voltage stability of an electric power system undergoes a deterioration when reactive power generation limits are reached [5]. Nevertheless, in most cases voltage stability remains when a unit reaches its reactive power generation limit (maximum or minimum). However, in highly loaded cases, sometimes the stability margin exhibits a discontinuous increase when a generator reaches its reactive power generation maximum or minimum limit, but the equilibrium point belongs to the unstable branches of the nose curves, hence the power system becomes immediately unstable due to any inevitable small perturbation, and a dynamic voltage collapse leading to blackout may follow.

Two methods to calculate the critical load margin have been presented in the literature ([4], [16]): continuation method and optimization method. The continuation method uses tangent vectors of the power flow equations to approach iteratively the saddle node bifurcation. This method provides a set of curves that show the evolution of the main characteristics of the power system: voltages (nose curves), reactive power generation, transmission losses, etc., with respect to the load margin [20]. The optimization methods formulate the problem as an optimization problem, with a linear objective function (the load margin) and nonlinear equality constraints (the augmented power flow equations). This method provides the Lagrange multipliers as sensitivities of the objective function (the load margin) with respect to the right hand side of the equality constraints (the augmented power flow equations). Those sensitivities become important in both corrective and preventive dispatch algorithms.

Preventive algorithms dispatch control resources to comply not only with N conditions (as corrective algorithms do) but also with N-1 security constraints.

The method selected to compute the voltages collapse point belongs to the continuation techniques family, thus the state variables manifolds from starting point to voltages collapse may be drawn. Precisely, the technique selected is a binary search where for each increment in the power dispatch control parameter λ, the corresponding solution x is attempted to be obtained. If solution exists, save the point and apply another power dispatch control parameter λ. If power flow is unfeasible for that power dispatch control parameter λ, the step is reduced. The process is considered finished when a minimum step is reached while the power dispatch control parameter λ is getting higher. A flow chart of the procedure is depicted in Figure 3-1.

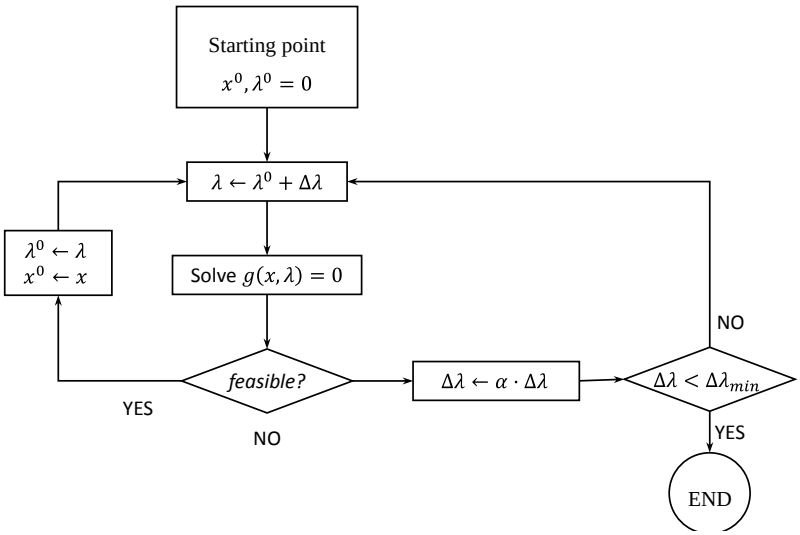

Figure 3-1: Flowchart of the computational procedure to determine the point of voltage collapse

Continuation approach has been chosen because it provides both the stability margin and a picture of the voltage variation as the load increases.

3.2. Illustrative examples

Large scale models of the Spanish and the French power systems have been used to test the proposed algorithms. Table 2.II has provided the features of them.

The distance to the voltage collapse will be determined assuming several generator and load models:

- Generator reactive power limits will be enforced (on) or relaxed (off)
- Constant reactive power loads and constant power factor loads

3.2.1. Spanish power system

Table 2.III has provided a summary of the operating point of the Spanish power system used as starting point.

Table 3.I illustrates the performance of the algorithm to determine the distance to the voltage collapse assuming two generator models (reactive power limits off and on) and two types of

load models (constant reactive load and constant power factor) in a model of the Spanish power system.

Obviously, the margin to voltage collapse becomes smaller if both generator reactive power limits and constant power factor loads are assumed.

The corresponding P-V curves are shown from Figure 3-2 through Figure 3-5: Spanish power system: P-V curves: reactive power generator limits on: constant PF load. P-V curves show the variation of the voltage magnitude of selected buses as the system demand increases. The voltage variation is computed and displayed until the point of voltage collapse which indicates the maximum loadability of the system. Four characteristic (pilot) buses of the Spanish power system have been chosen. It must be noted that the shape of the voltage variation depends on the selected bus. 'VIC' bus, which is the Spanish terminal of one of the tie-lines between France and Spain exhibits the largest voltage excursion.

Table 3.I. Spanish power system: Margin to voltage collapse

	INITIAL	FINAL (QGlimits off)		FINAL (QGlimits on)	
Constant Q load	40612	58888	(+45.0 %)	51044	(+25.7 %)
Constant PF load	40612	56603	(+39.4 %)	49354	(+21.5 %)

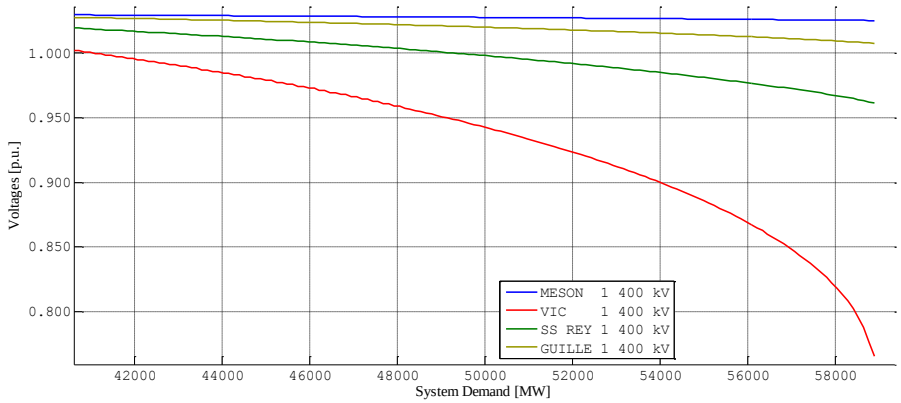

Figure 3-2: Spanish power system: P-V curves: reactive power generator limits off: constant Q load

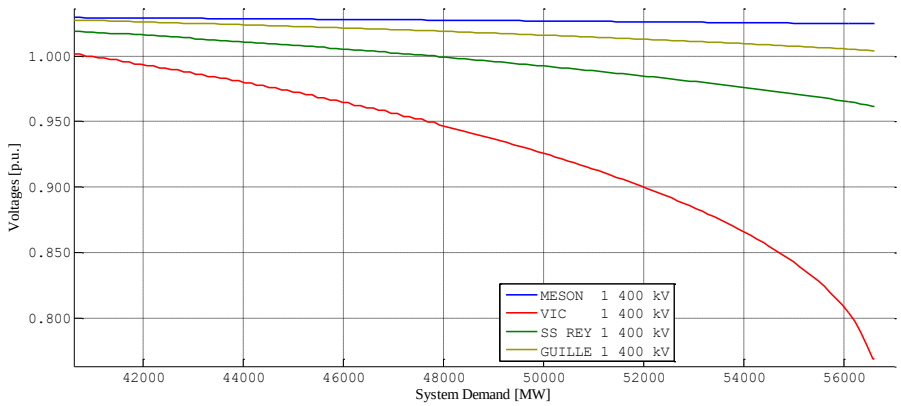

Figure 3-3: Spanish power system: P-V curves: reactive power generator limits off: constant PF load

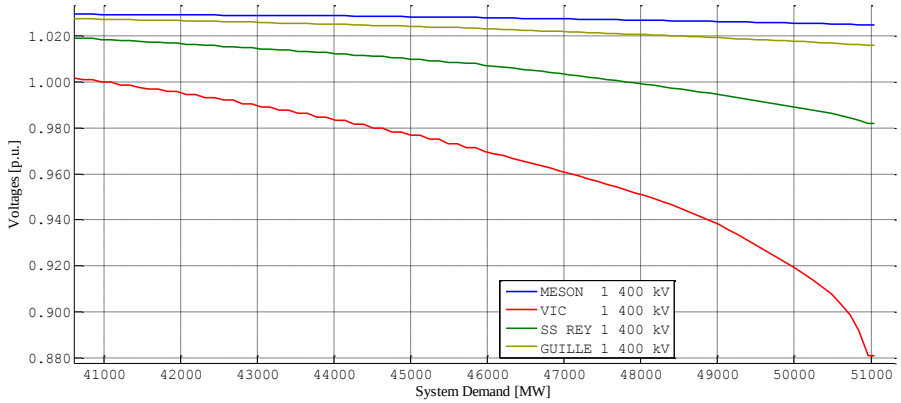

Figure 3-4: Spanish power system: P-V curves: reactive power generator limits on: constant Q load

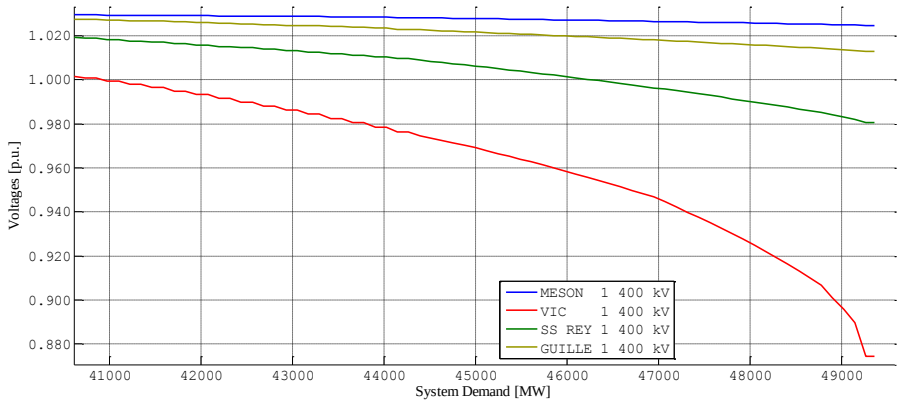

Figure 3-5: Spanish power system: P-V curves: reactive power generator limits on: constant PF load

3.2.2. French power system

Table 2.VII has provided a summary of the operating point of the French power system used as starting point.

Table 3.II illustrates the performance of the algorithm to determine the distance to the voltage collapse assuming two generator models (reactive power limits off and on) and two types of load models (constant reactive load and constant power factor) in a model of the French power system.

Obviously, the margin to voltage collapse becomes smaller if both generator reactive power limits and constant power factor loads are assumed.

The corresponding P-V curves are shown from Figure 3-6 through Figure 3-9.

The voltage variation is computed and displayed until the point of voltage collapse which indicates the maximum loadability of the system. Four characteristic (pilot) buses of the French power system have been chosen. It must be noted that the shape of the voltage variation depends on the selected bus. In contrast to the Spanish power system, the displayed bus voltage variations are very similar.

Table 3.II. French power system: Margin to voltage collapse

	INITIAL	FINAL (QGlimits off)		FINAL (QGlimits on)	
Constant Q load	102134	136939	(+34.1 %)	114725	(+12.3 %)
Constant PF load	102134	135695	(+32.9 %)	113504	(+11.1 %)

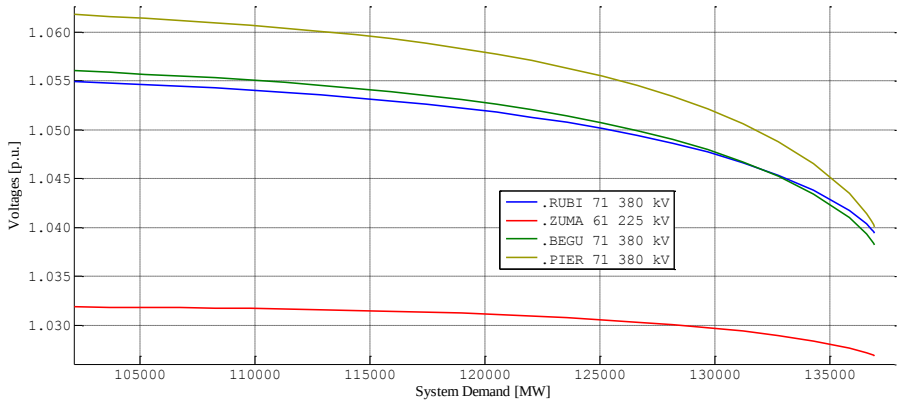

Figure 3-6: French power system: P-V curves: reactive power generator limits off: constant Q load

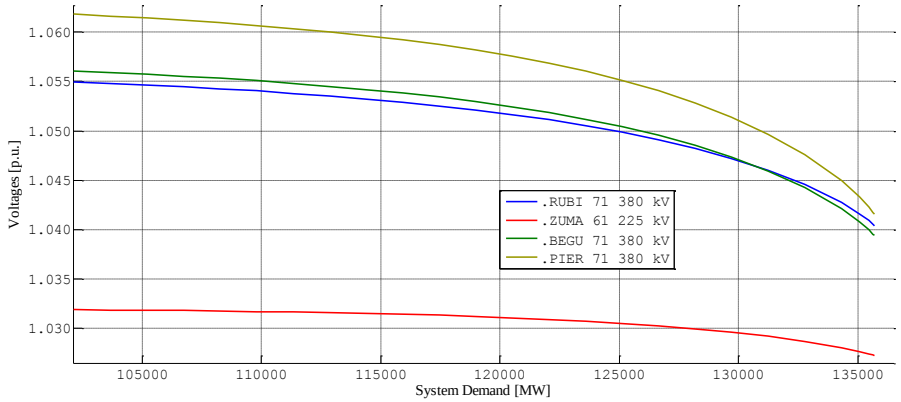

Figure 3-7: French power system: P-V curves: reactive power generator limits off: constant PF load

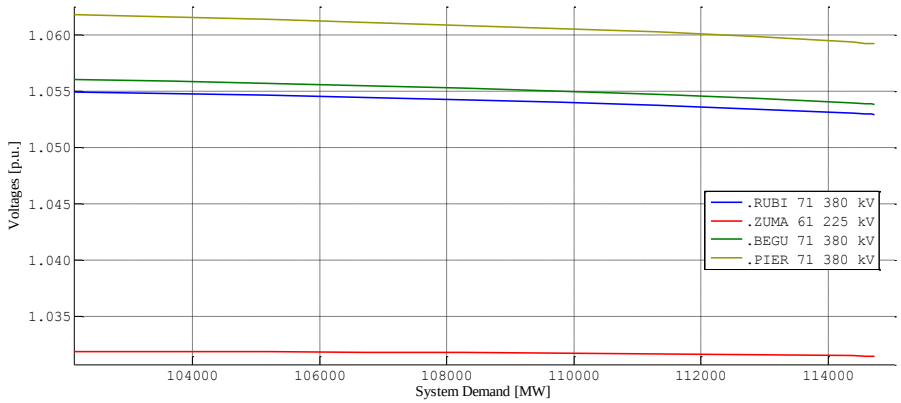

Figure 3-8: French power system: P-V curves: reactive power generator limits on: constant Q load

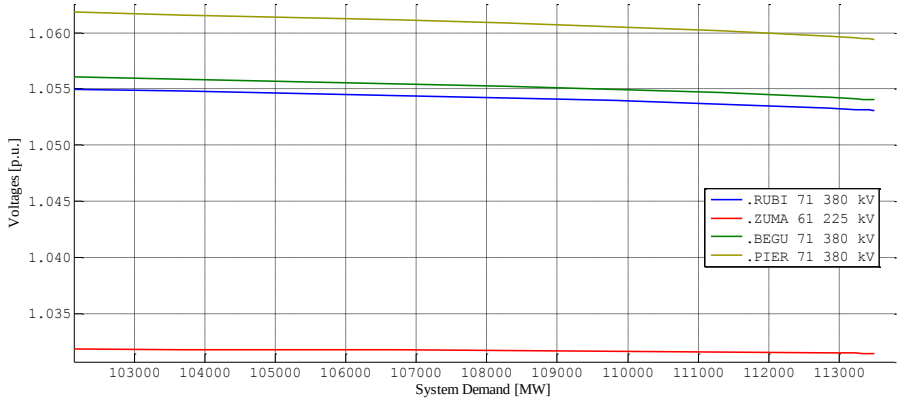

Figure 3-9: French power system: P-V curves: reactive power generator limits on: constant PF load

3.3. Partial conclusions

The flexibility and robustness of the algorithm to assess voltage stability of large power systems has been shown. The maximum load that generators can serve (or the maximum loadability of the power system) has been determined. The voltage stability of a power system has been measured using the distance to the point to maximum loadability of the power system or point of voltage collapse.

4. Impact of models and controls of wind generators and HVDC links on system performance

Transient and small-signal stability analyses not only need the steady-state model of the network provided by an AC load flow, but also the dynamic model of generators and other dynamic devices. Simplified models of synchronous generators have been used instead of detailed models whenever those models are not available. In addition to synchronous generators models, wind generator and HVDC links might have to be added. Hence, it has to be investigated if simplified models of wind generators and HVDC links can be used. The investigation consists in determining the impact of models and controls on the transient stability of a small-scale test system.

Transient stability is quantified by the critical clearing time of a fault, i.e., the maximum duration of the fault for which the power system does not turn unstable. Figure 4-1 illustrates transient instability due to the loss of synchronism. The system turns unstable when the relative angles after clearing the fault do not return to their initial values but instead continue diverging. The evolution of the relative angles is observed in order to determine system instability. Since instability is usually tantamount to a continuous, non-oscillatory increase of relative angles, a critical angle is imposed. If one relative angle exceeds this critical angle, the system is deemed unstable and the critical clearing time exceeded.

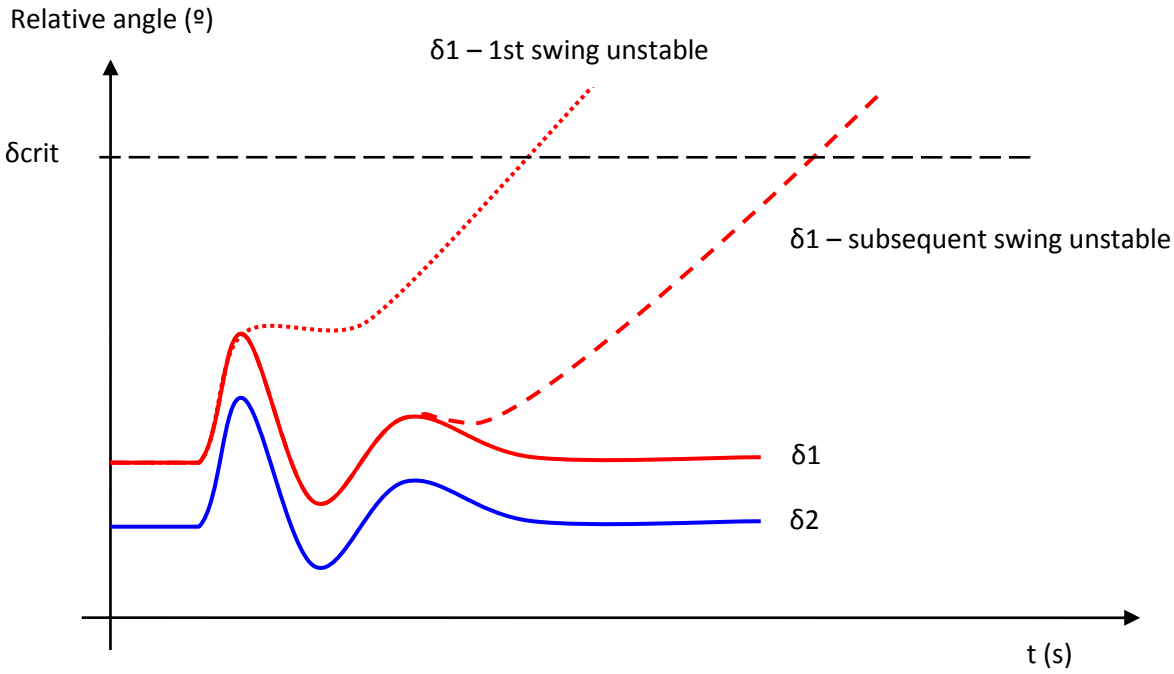

Figure 4-1 : Transient instability due to loss of synchronism

4.1. Small-scale test systems

A small-scale test system proposed for fundamental studies of power system stability [4] has been considered (see Figure 4-2). It comprises two areas, four generators and eleven buses.

There are two generators in each area. There is a weak link between the two areas. The link is used to transmit power from the exporting area to the importing one.

A test two-area system with wind generators and one HVDC link of LCC and VSC technologies has been used (see Figure 4-3) to draw conclusions related to the impact of their control schemes in the system performance.

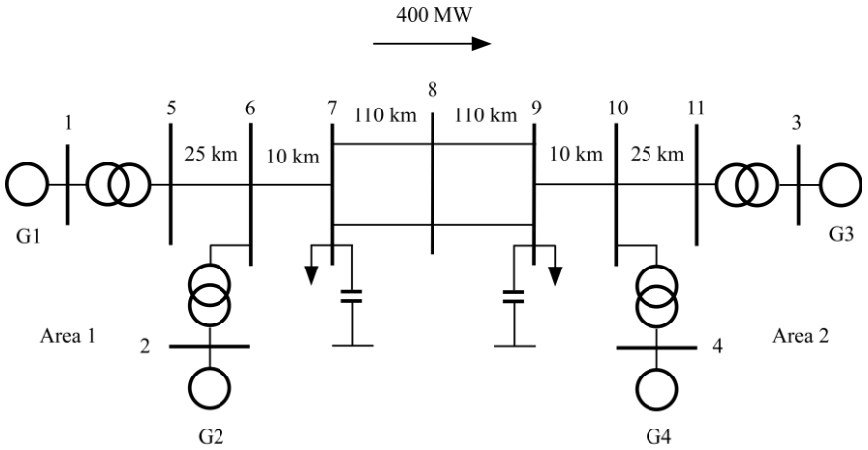

Figure 4-2. Two-area test system

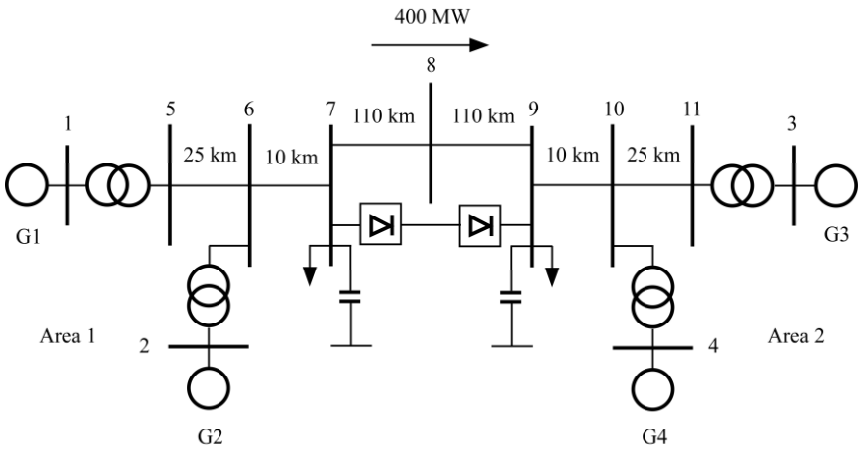

Figure 4-3. Two area test system with HVDC link

The impact of control schemes of wind generators and HVDC links on the critical clearing time of a solid three phase fault at the midpoint bus (8) is investigated.

4.2. Impact of wind generator models on transient stability

4.2.1. Wind generator model

A simplified model valid for DFIG and MSG wind generators has been developed. It implements the response required by TSOs in grid codes [5]. It comprises:

- Controllable current source implemented as a load model (see Figure 4-4)
- Current limiter (see Figure 4-5)
- Converter (see Figure 4-6)
- P-f control (see Figure 4-7), and
- V-Q control (see Figure 4-8)

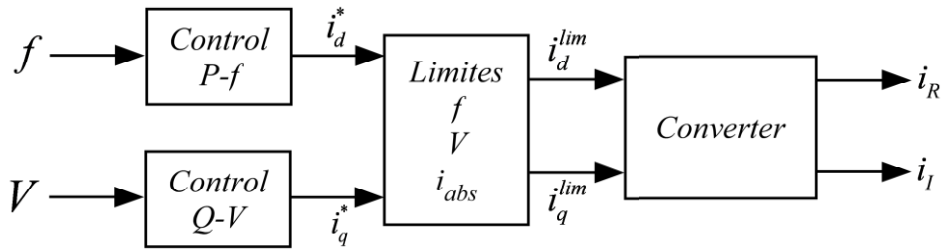

Figure 4-4. Wind generator model: Controllable current source

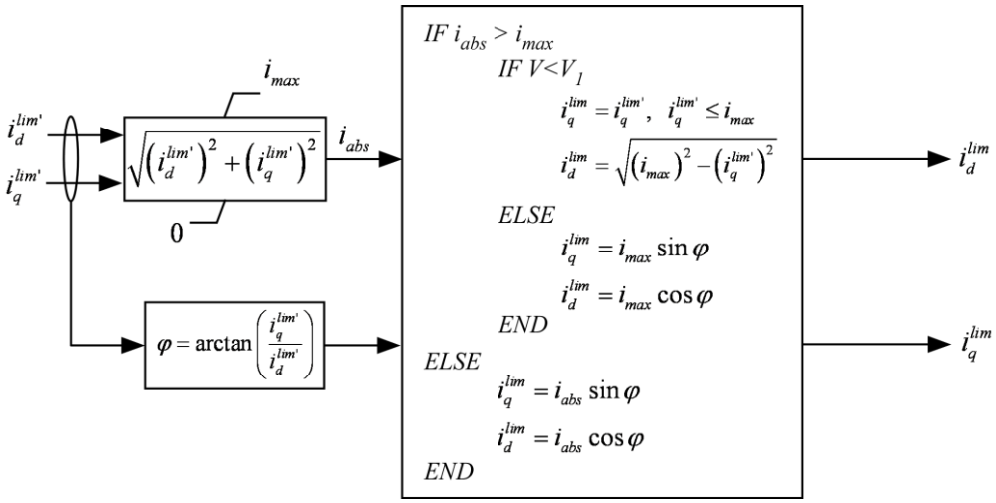

Figure 4-5 : Current limiter

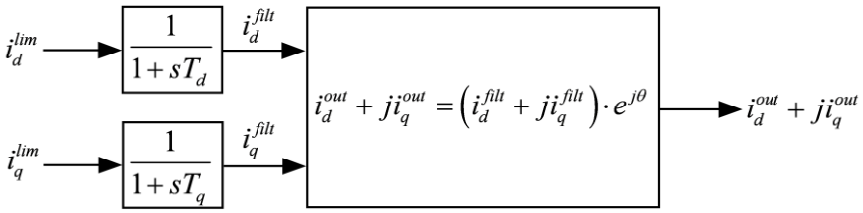

Figure 4-6 : Converter

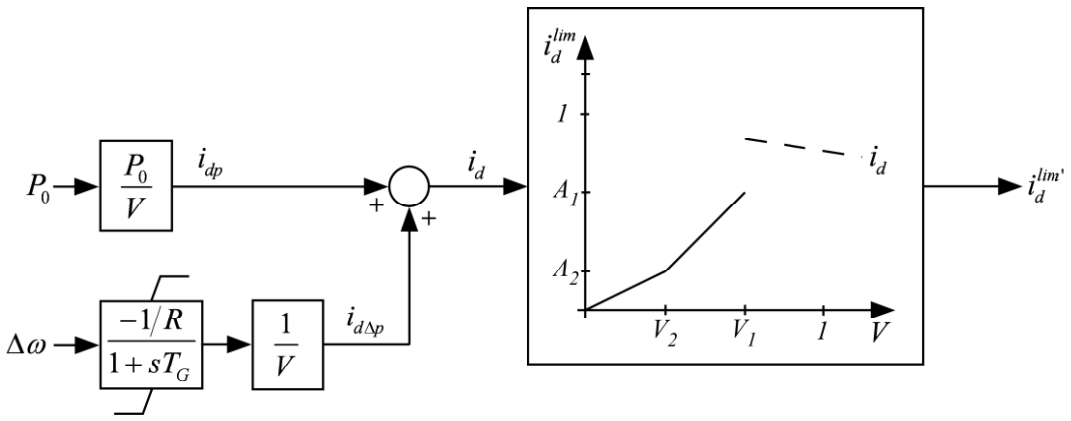

Figure 4-7. Wind generator model: P-f control

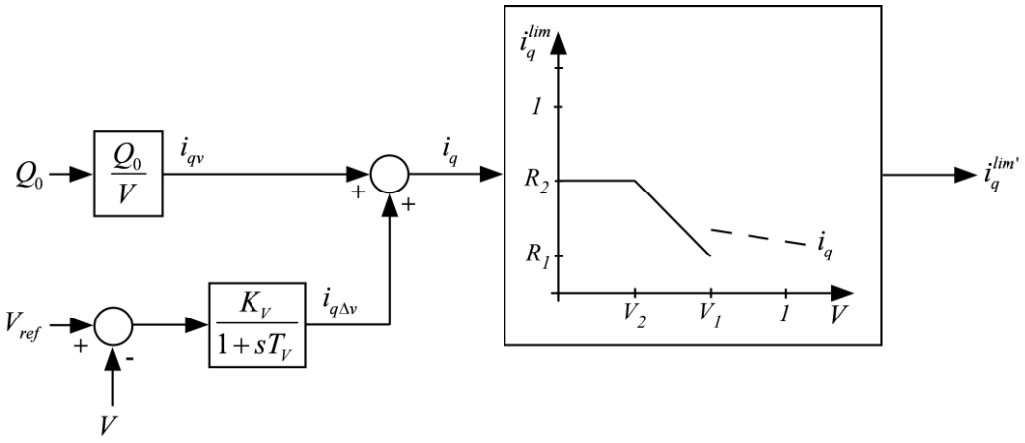

Figure 4-8. Wind generator model: Q-V control

4.2.2. Simulation results

The impact of substituting synchronous generators by wind generator and of the modeling degree of wind generators is addressed. Five test cases are considered:

- The original test case in which all generators are synchronous ones.
- Generators 2 and 4 have become wind generators. Wind generators have been represented by fully detailed models.
- Generators 2 and 4 have become wind generators. Wind generators have been represented by oversimplified (constant current) models.
- Generator 2 has become wind generators. Wind generator has been represented by fully detailed model.
- Generator 4 has become wind generators. Wind generator has been represented by fully detailed model.

Figure 4-9 shows synchronous generator rotor angles in terms of critical clearing time of the original two-area system (0.99 s). Figure 4-10 shows synchronous generator rotor angles in terms of critical clearing time of the two-area system with two wind generators. There are only two synchronous generators in this case.

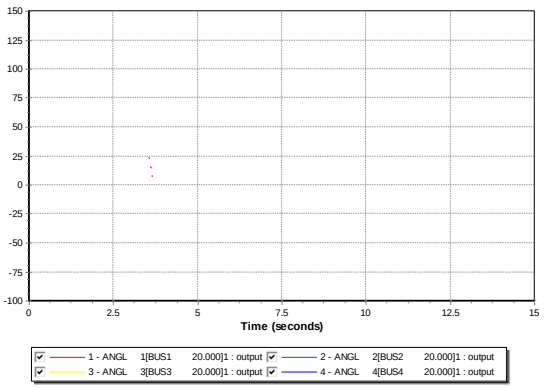

Figure 4-9. Response of the original two-area test system in terms of the critical clearing time: generator rotor angles

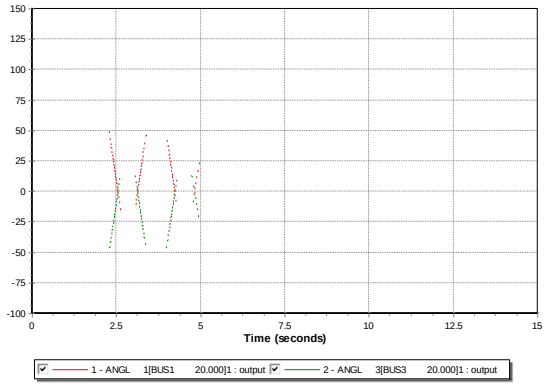

Figure 4-10. Response of the two-area test system with two wind generators in terms of the critical clearing time: generator rotor angles

Table 4.I compares the critical clearing times of the five test cases considered.

Table 4.I. Impact of control schemes of wind generators on the critical clearing time

Wind generators	
Original	0.99
With WGs	0.62
Oversimplified	0.865
Without V-Q control	1.095
WG at 2	0.64
WG at 4	0.82

The study has shown that not only substituting synchronous generators by wind generators has a substantial impact on power system stability but the modelling degree and control configuration affect it as well. Omitting V-Q control of wind generators (see Figure 4-8) seems to be beneficial in terms of critical clearing time. The location of wind generation also influences transient stability significantly, although without improving the original case. Wind generators with V-Q control located in the importing area improve critical clearing time with respect to the case where wind generators are located in both areas.

4.3. Impact of HVDC link models on transient stability

Models of LCC and VSC links are available within PSS/E model library ([6], [7]). They will be used in this study.

Converters of LCC-HVDC links are usually made of three-phase thyristor bridges [4]. Turn-off of thyristors can be controlled by the so-called firing angle. The firing angles of the converters at each terminal of the HVDC link in turn depend on the supervisory control, where one converter (the inverter) controls the dc-link voltage and the other (the rectifier) controls the dc-link current. Thyristor bridges always absorb reactive power and hence active and reactive power control is coupled.

Converters of VSC-HVDC links are usually built of three-phase bridges of self-commutating devices such as IGBT or GTO. Turn-on and turn-off is realized by pulse-width modulation (PWM) schemes (e.g, sinusoidal or space-vector PWM). The PWM schemes are fed by signals from the current control loops, which in turn depends on external control loops on active power and reactive power [8], [9]. On terminal controls the active power, whereas the other

controls the dc-link voltage. Active and reactive power controls are decoupled. Additionally, reactive power at each terminal can be controlled independently.

Table 4.II shows a comparison of LCC- and VSC-HVDC links.

Table 4.II. Comparison of LCC- and VSC-HVDC link

LCC HVDC	VSC HVDC
High power capability (Thyristor)	Lower power capability (IGBT)
Good overload capability	Weak overload capability
Need for strong AC system	Operates into weaker AC systems
Limited black start capability	Black start capability
Harmonic distortion	Insignificant harmonic distortion
Coarse reactive power control	Finer reactive power control
Large site	50% site requirements of LCC
Lower station loss	Higher station loss
Lower cost	Higher cost
Mature	Less mature
MI cables (higher voltage capability)	XLPE cables (lower voltage capability)

4.3.1. LCC-HVDC model

Figure 4-11 shows the principles of the converter control of LCC-HVDC links in PSS/E ([6], [7]). The rectifier controls the dc-link current by adjusting its firing angle, whereas the inverter adjusts its firing angle to control the dc-link voltage. However, firing angles α and γ of the rectifier and the inverter respectively are restricted to certain values around 15-20º, with a minimum firing angle α of 5º. Tap changer control is used to keep the converter firing angles within the desired range. Converter operation is also restricted by the maximum and minimum allowable currents and voltages. Figure 4-12 displays the block diagram representation of the model of LCC-HVDC link converter.

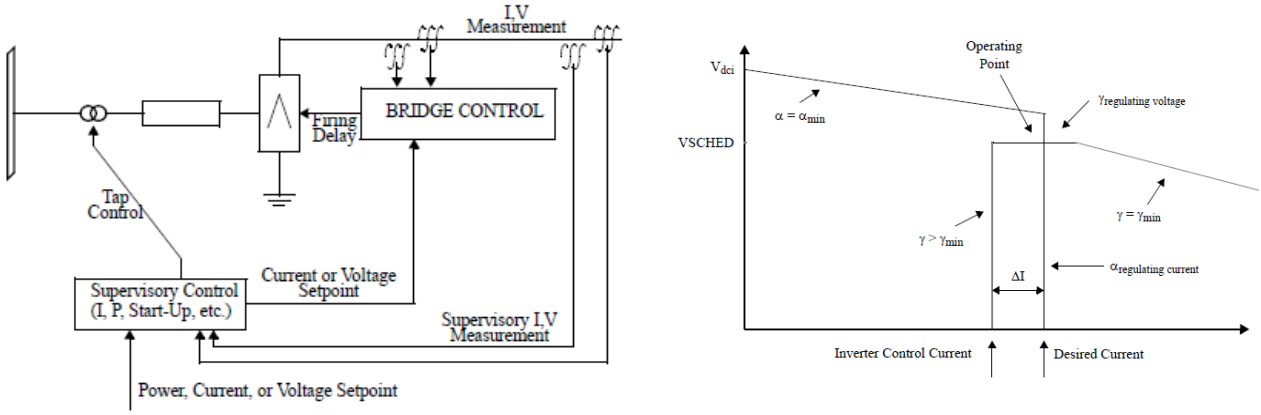

Figure 4-11 : LCC-HVDC converter control principles

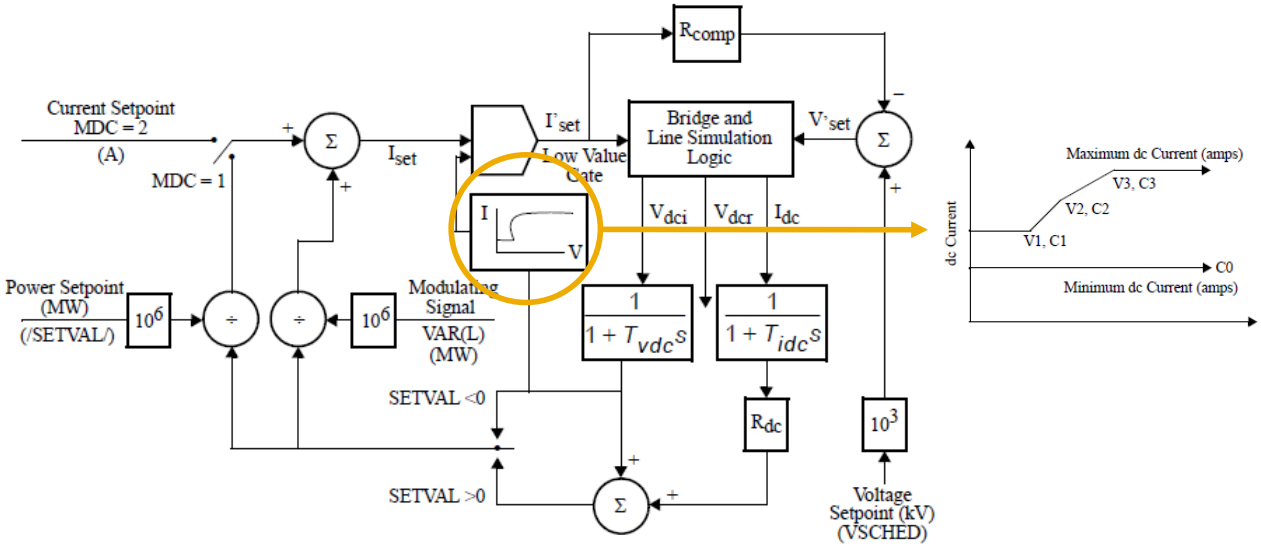

Figure 4-12 : LCC-HVDC converter control model

4.3.2. VSC-HVDC model

Figure 4-13 shows the principles of the converter control of VSC-HVDC links in PSS/E. Both converters are current controlled. Current control is carried out in rotating reference system by applying a Park transform. Current set points depend on the external control loops. One converter controls the dc-link voltage, whereas the other controls the active power flow. Reactive power control loop of VSC HVDC links can be set to control either reactive power or AC voltage. Converter operation is restricted by current and voltage limits. Figure 4-14 displays the block diagram representation of the model of VSC-HVDC link converter. Figure 4-15 provides the current limiter of VSC-HVDC link converter model.

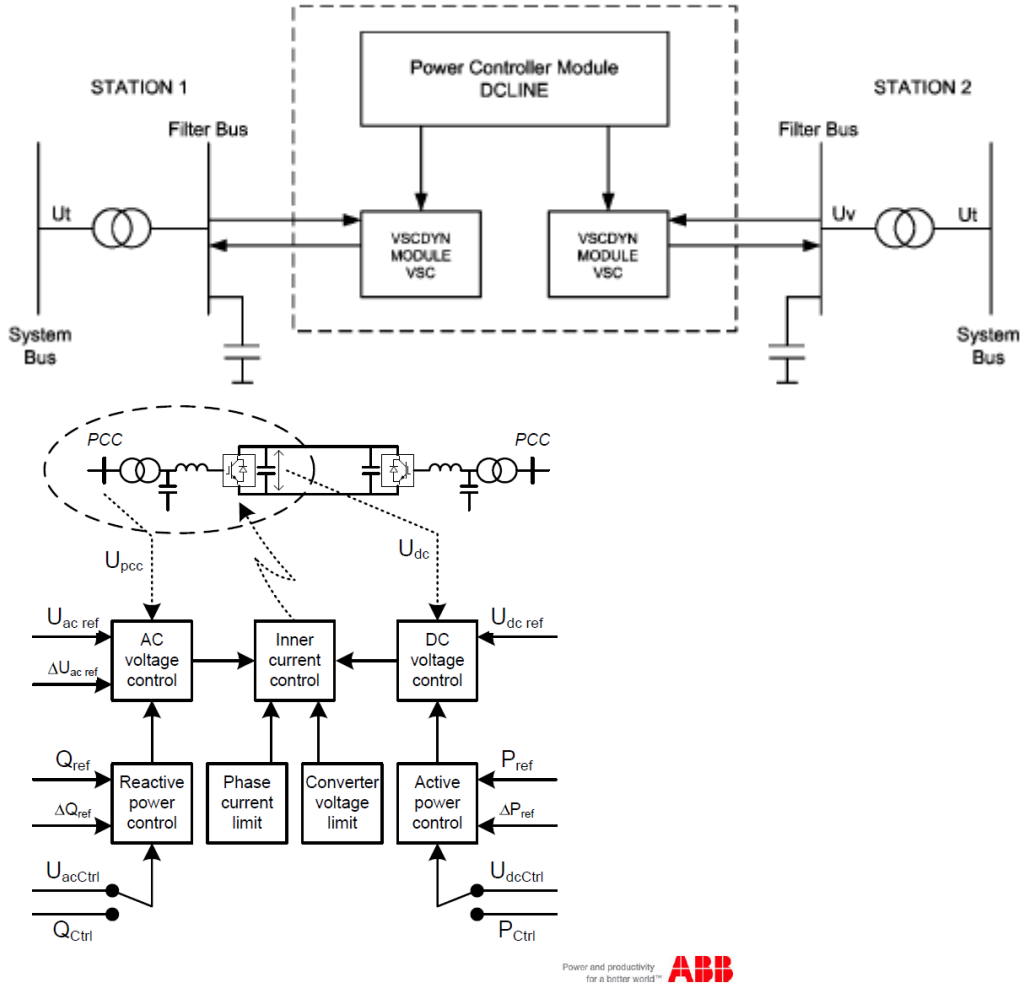

Figure 4-13: VSC-HVDC converter control principles

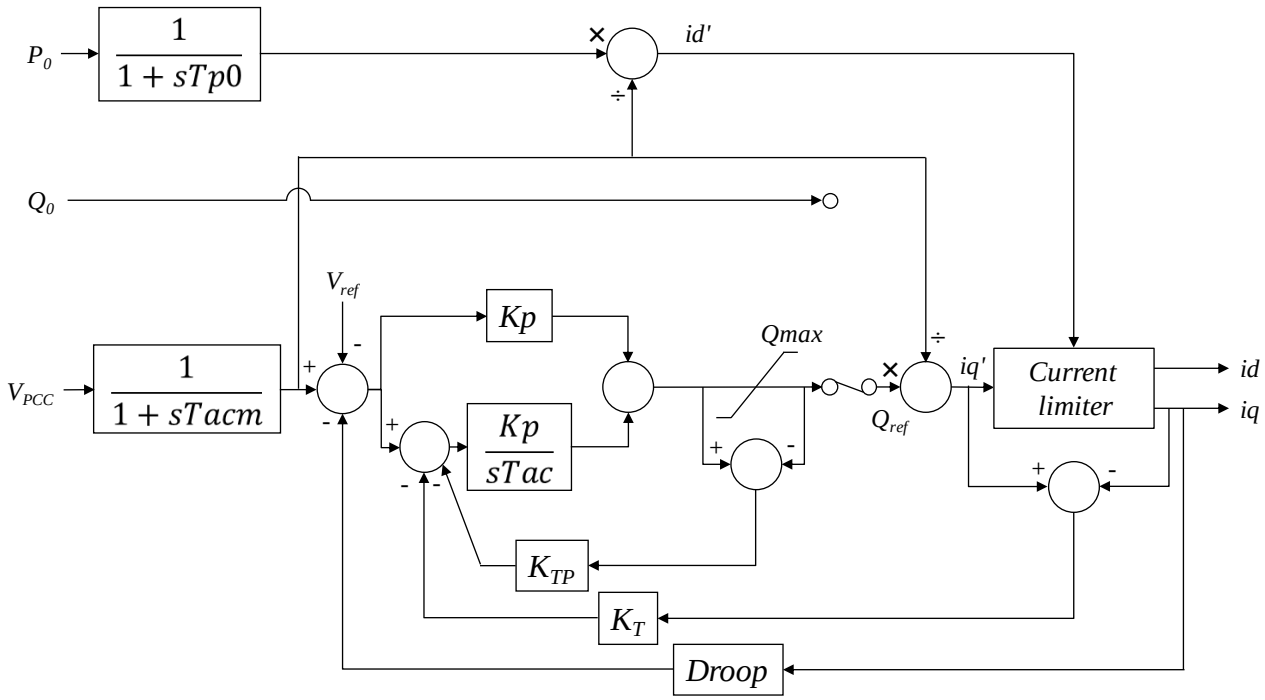

Figure 4-14: VSC-HVDC converter control model

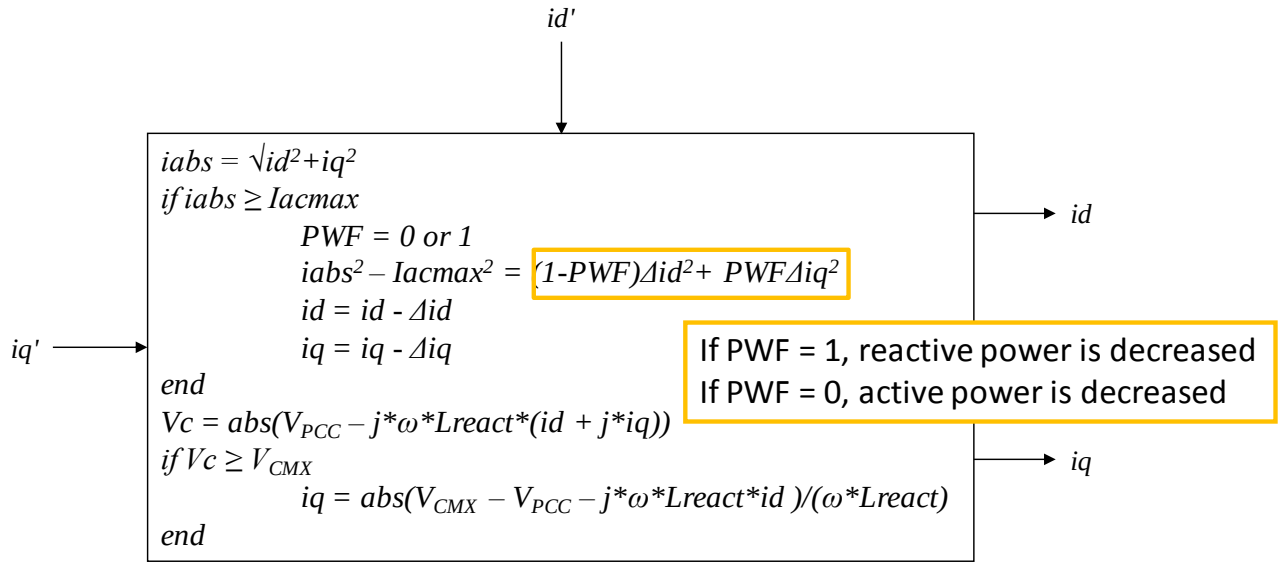

Figure 4-15: VSC-HVDC converter control model: current limiter

4.3.3. Supervisory controls

Figure 4-16 shows the investigated DC power and reactive power set point modulation strategies. The former depends on the frequency difference of the two terminals as for example suggested in [10], whereas the latter depends on the difference of each terminal's frequency and the average frequency of both terminals. Average frequency is used to obtain a rough estimation of the frequency of the centre of inertia a two-area system interconnected by a HVDC link. Note that reactive power modulation only applies to VSC HVDC links unless LCC HVDC links are equipped with thyristor controlled reactors and capacitors.

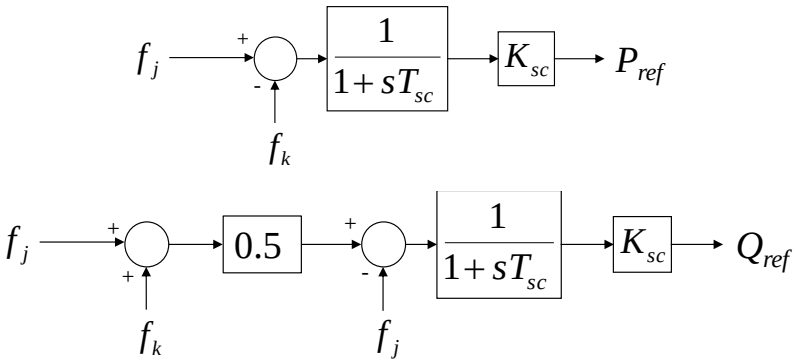

Figure 4-16. Active and reactive power set point modulation

In steady state operation, frequency deviations and differences are zero and consequently active and reactive power set points remain constant. In transient operation, active and reactive power set points are modulated as shown in Figure 4-16. The distinction between using terminal frequency differences and the difference of the terminal frequencies and the average frequency influences the impact on transients. Actually, the latter is able to distinguish accelerating and decelerating areas and reactive power set points of opposite signs are applied to accelerating-side and decelerating-side VSC HVDC link terminals.

4.3.4. Simulation results

The impact of incorporating an LCC-HVDC links on the critical clearing time of solid three phases fault at the midpoint bus of AC tie line is investigated firstly.

Table 4.III provides the critical clearing time of the test case with parallel LCC-HVDC link. The critical clearing time has increased from 0.99 s to 1.175 s.

Table 4.III. Impact of LCC-HVDC links on the critical clearing time

LCC-HVDC	
Original	0.99
With HVDC	1.175

Figure 4-17 displays the power flow in the AC line in terms of critical clearing time of the original two-area system. Figure 4-18 shows the power flow in the AC line in terms of critical clearing time of the two-area system with the LCC-HVDC link. The LCC-HVDC link almost maintains the power flow during the fault.

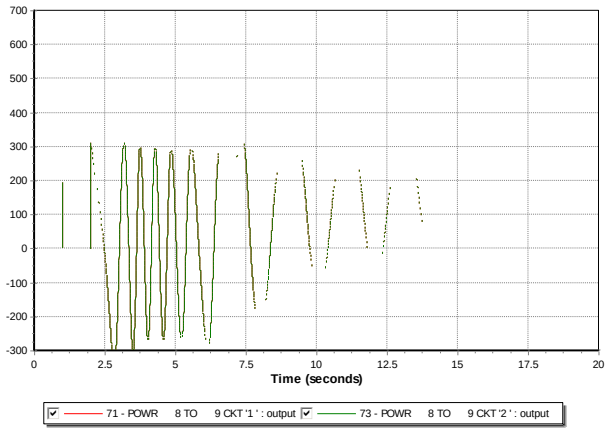

Figure 4-17. Response of the original two-area test system in terms of the critical clearing time (green curve: power through AC line)

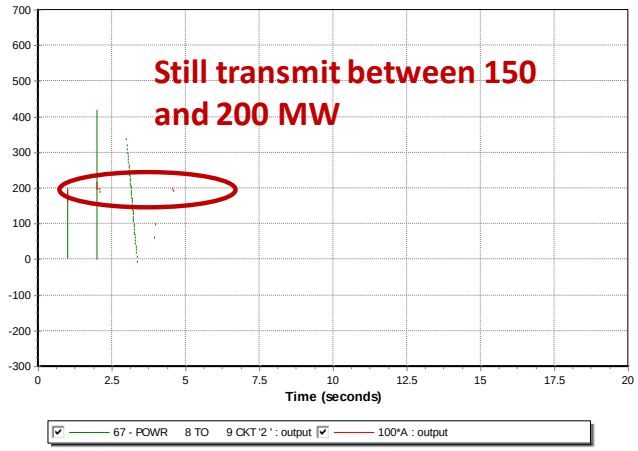

Figure 4-18. Response of the two-area test system with LCC-HVDC link (green curve: power through AC line; red curve: power through the HVDC link)

Table 4.IV provides the critical clearing times of the test case with parallel VSC-HVDC link under different control schemes. All control schemes except one result in higher critical clearing times than the original one (0.99 s). It is interesting to see that reactive power control of the terminal converters yields to better results than voltage control. Further, in case of current

limits are hit, it is detrimental to reduce the active power component of the current, reducing inter-area power flow. Finally, voltage control at the terminal within the exporting area (bus 7) and reactive power control at the terminal within the importing area (bus 9) improves further the critical clearing time. This is mainly due to the fact that voltage control keeps voltages high at the exporting area, slowing down acceleration with respect to the importing area, whereas reactive power control keeps reactive power constant, maintaining voltages low at the importing area during the fault.

Table 4.IV. Impact of control schemes of VSC-HVDC links on the critical clearing time

VSC-HVDC	
Original	0.99
V-control: decrease P	0.585
V-control: decrease Q	1.13
Q-control: decrease P	1.38
Q-control: decrease Q	1.38
V-control at 7, Q-control at 9	2.165

Figure 4-19 shows the power flow in the AC line in terms of critical clearing time of the two-area system with the VSC-HVDC link. The VSC-HVDC link maintains the power flow during the fault.

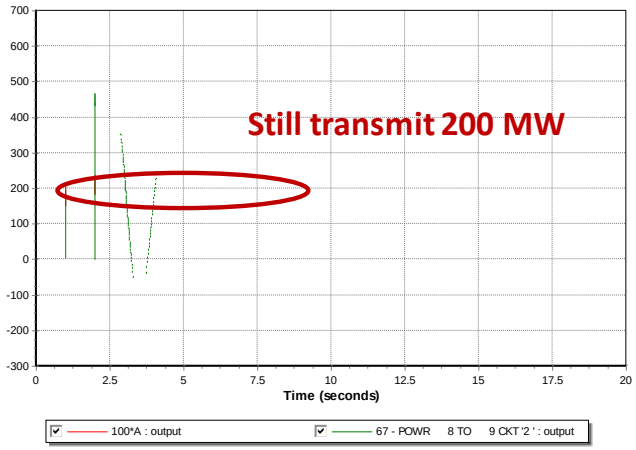

Figure 4-19. Response of the two-area test system with VSC-HVDC link (green curve: power through AC line; red curve: power through the HVDC link)

4.4. Partial conclusions

The investigation has found that the impact of models and controls of wind generators and HVDC links on the transient stability of a small-scale test system is significant. Hence, simplified models of power system components should be avoided.

Moreover, it has been found that some controls contribute to improve the transient stability of the power system, whereas other controls deteriorate it. Therefore, robustness of grid architectures would rely on appropriate control schemes, that is, those schemes which enhance power system transient stability.

Part of the results of this investigation have been summarized in the paper “A fundamental study on the impact of HVDC lines on transient stability of power systems” by L. Sigrist, F.

Echavarren, L. Rouco and P. Panciatici that has been accepted for presentation at the IEEE Power Tech 2015.

5. Transient stability analysis

5.1. Study method

Transient stability is concerned with the ability of synchronous generators to remain in synchronism is case of a fault. Transient stability is assessed simulating in the time domain the non-linear differential equations that describe power system behavior. Several compute tools are available. We will use a tool widely used worldwide, including Europe: PSS/E ([6], [7]).

Transient and small-signal stability analyses not only need the steady-state model of the network provided by an AC load flow, but also the dynamic model of generators and other dynamic devices.

Simplified models of synchronous generators have been used instead of detailed models whenever those models are not available (typically due to confidentiality reasons). The simplest model of a synchronous generator is the so called classical model. The classical model comprises the rotor dynamics and simplified electrical model of the synchronous machine (voltage source behind the transient reactance which magnitude is constant and which angle is the rotor angle).

In addition to synchronous generators models, wind generator and HVDC links might have to be added. We have found the relevance of not only detailed models of wind generators and HVDC links but also of their control schemes.

Hence, we suggest using typical models of synchronous generator components. Typical models can be proposed for each generating unit technology. Generating unit technologies are nuclear, thermal, gas, hydro, wind, solar thermal and solar photovoltaic.

5.1.1. Dynamic models of generator components

Typical (PSS/E) models will be assumed according to the generating unit technology ([6], [7]):

- Nuclear (GENROU, EXCA1, TGOV3)
- Thermal (GENROU, EXAC3, IEEEG1)
- Combined cycle (GENROU, ESST4B, PSS2A, GAST2A)
- Gas (GENROU, EXCAC1, GAST2A)
- Hydro (GENSAL, ST6B, PSS2A, HYGOV)
- Wind (User model)
- PV solar (User model)

GENROU model corresponds to a round rotor synchronous machine. GENSAL model represents salient pole synchronous machine. GENROU and GENSAL correspond to models IEEE, models 2.2 and 2.1 respectively [11].

Figure 5-2, Figure 5-4, Figure 5-3 and Figure 5-4 display respectively EXAC1, EXAC3, ESST4B and ST6B PSS/E excitation system models. EXAC1 and EXAC3 models represent alternating current (AC) excitation systems. AC excitation systems use a synchronous generator as main exciter. ESST4B and ST6B models represent static excitation (ST) systems. ST excitation systems use a thyristor bridge as main exciter. Figure 5-5 shows PSS/E PSS2A stabilizer model. PSS2A is a dual input power system stabilizer.

Models of excitation systems and power system stabilizers for power system stability studies have been developed by IEEE for many years and incorporated to a standard (see [12]). IEEE models of excitation systems are incorporated to model libraries of power system simulation programs by program developers.

Figure 5-7, Figure 5-6, Figure 5-7, Figure 5-8, Figure 5-10 and Figure 5-9 depict TOGV3, IEEEG1, GGOV1, GAST2A and HYGOV PSS/E turbine governor models.

Models of turbine governors for power systems stability studies have been developed by IEEE for many years. References [13], [14] and [15] describe respectively models of steam, gas and hydro turbines proposed by IEEE. Models are incorporated to model libraries of power system simulation programs by program developers.

The wind generator model has been described in section 4.2.1. This model is also used to represent solar PV plants.

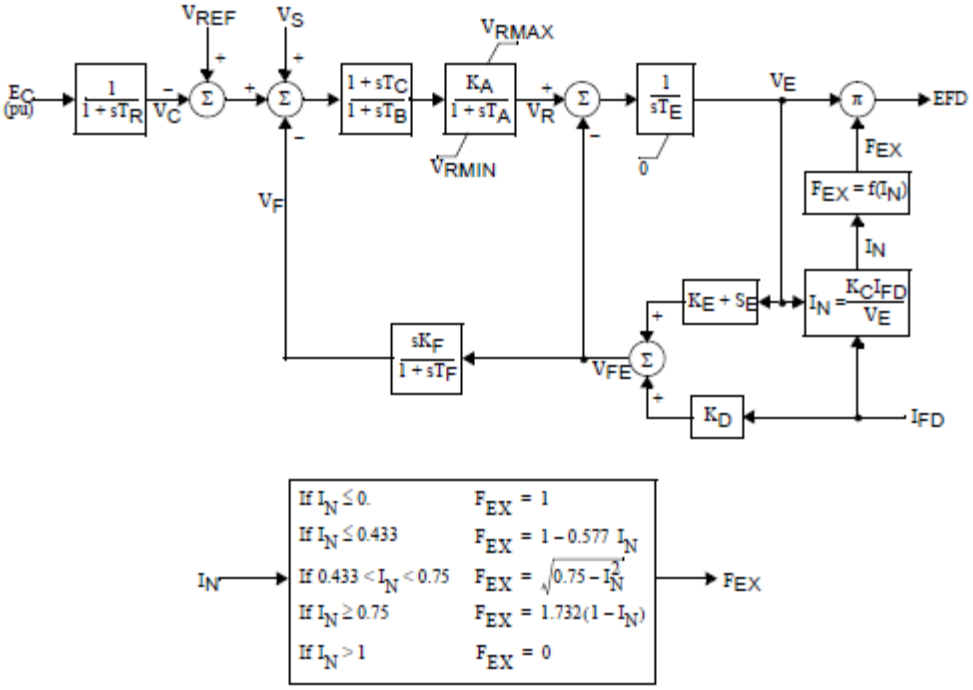

Figure 5-1: PSS/E EXAC1 excitation system model

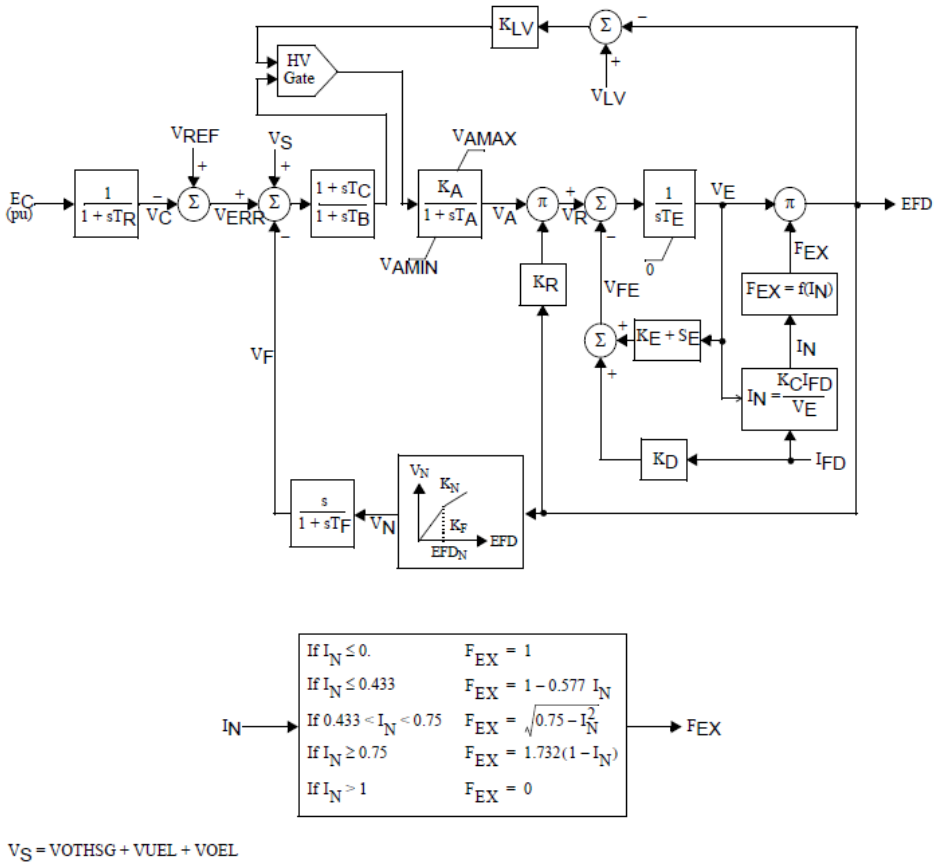

Figure 5-2: PSS/E EXAC3 excitation system model

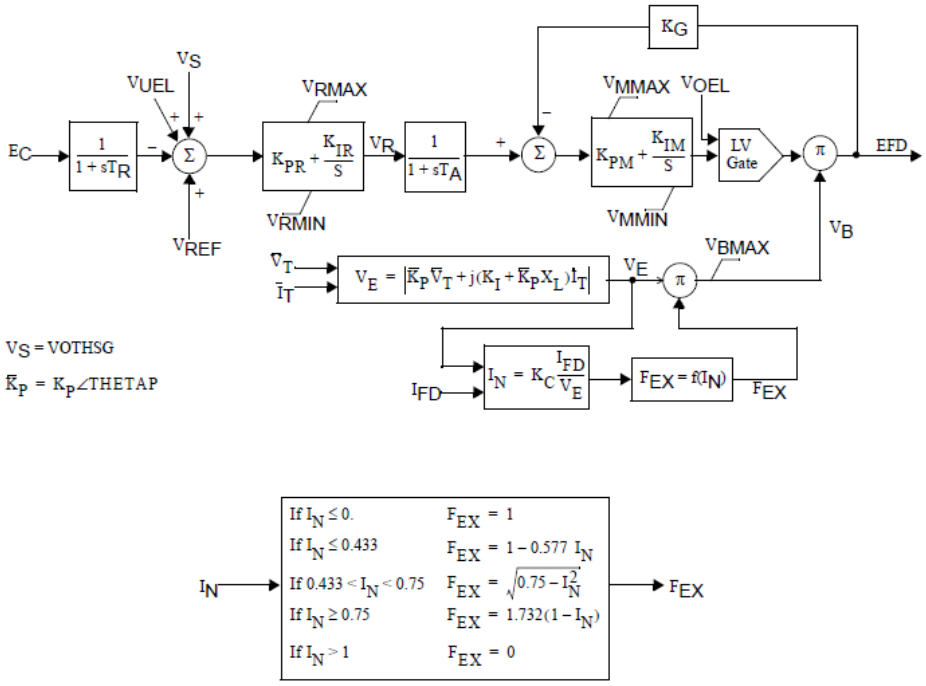

Figure 5-3: PSS/E ESST4B excitation system model

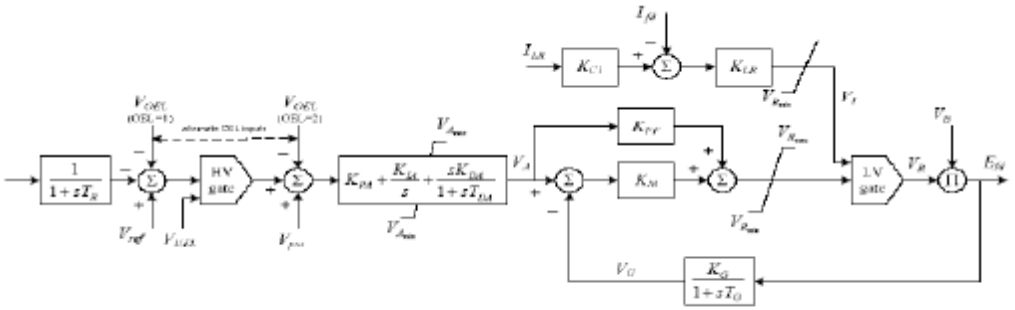

Figure 5-4: PSS/E ST6B excitation system model

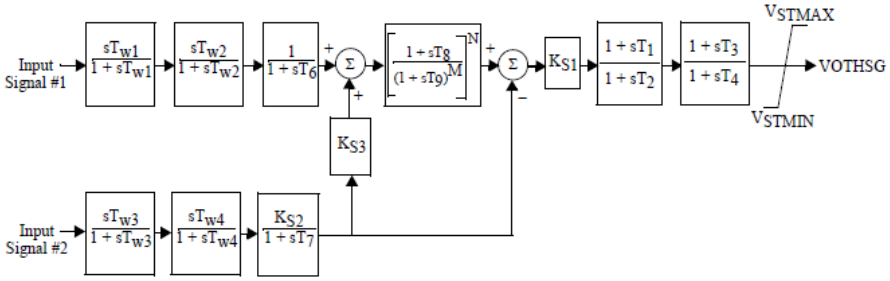

Figure 5-5: PSS/E PSS2A stabilizer

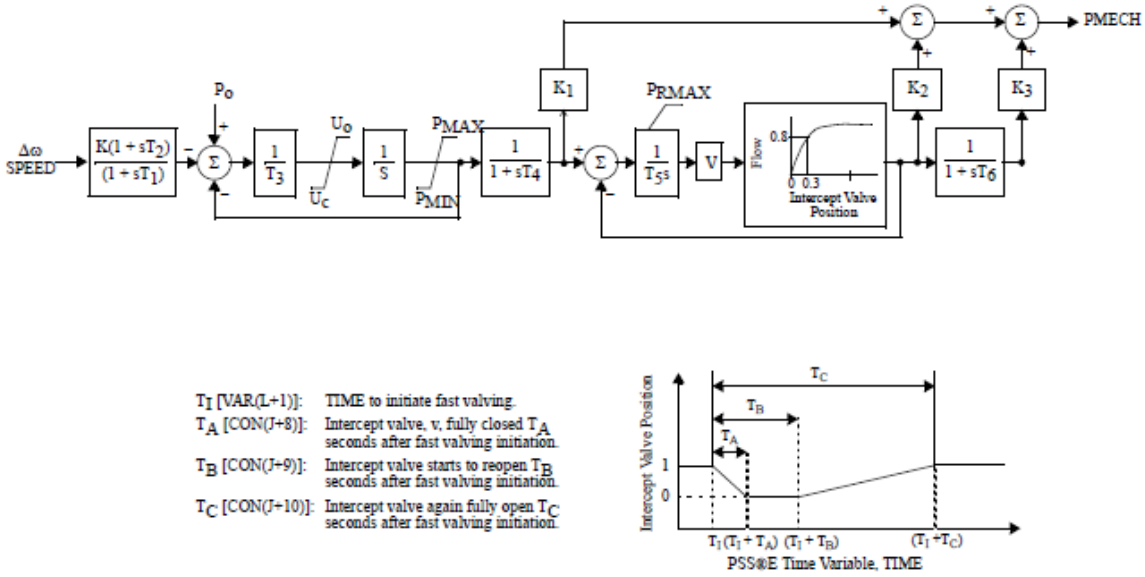

Figure 5-6: PSS/E TGOV3 turbine and governor

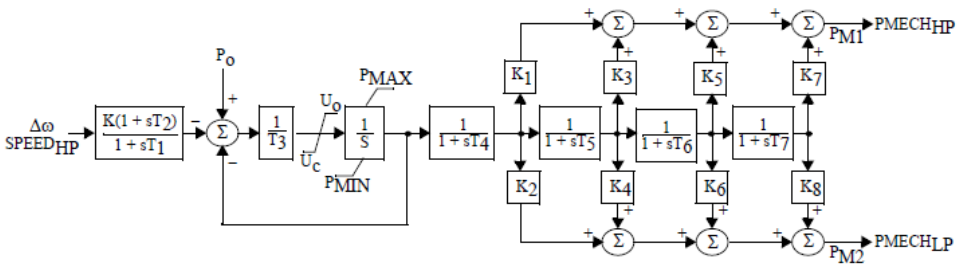

Figure 5-7: PSS/E IEEEG1 turbine and governor

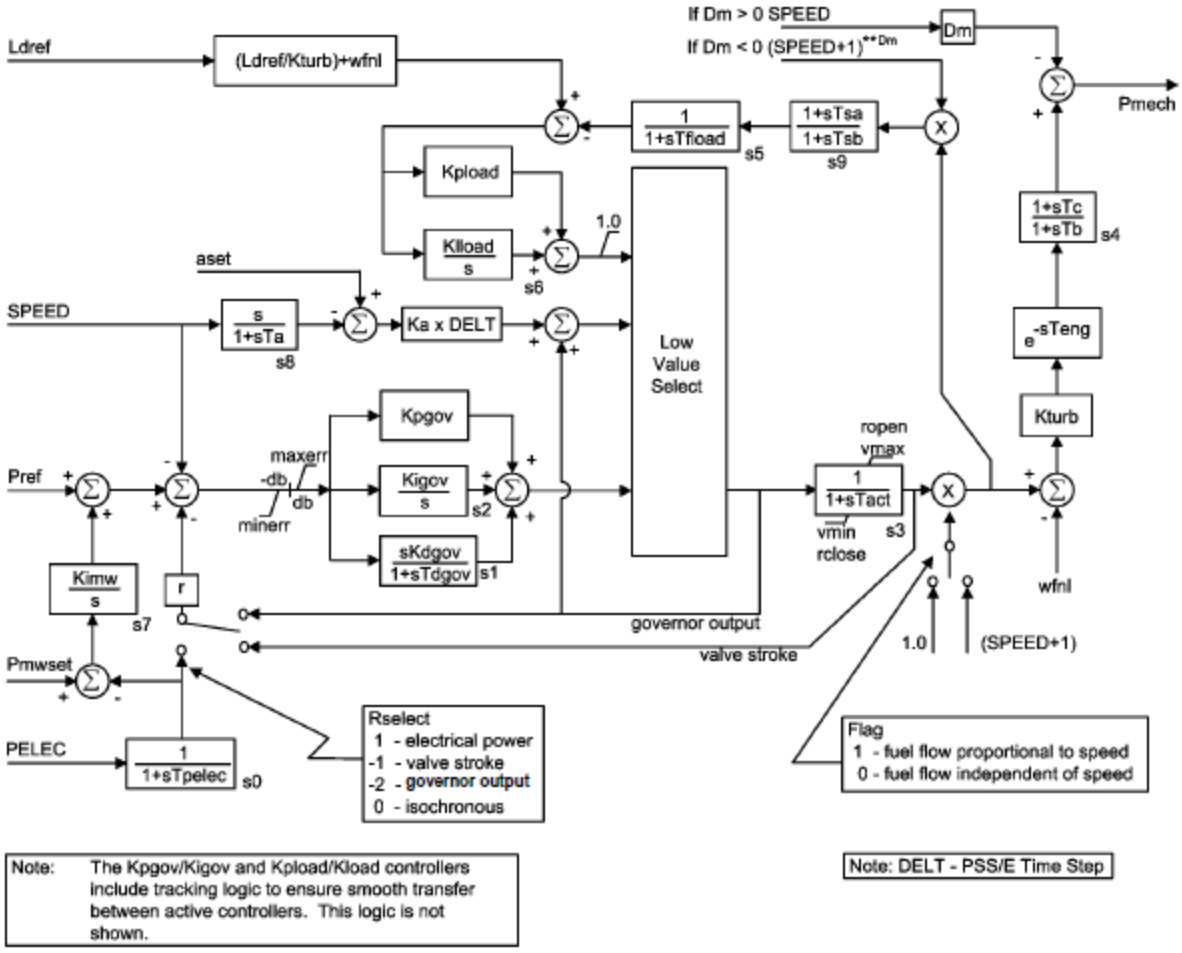

Figure 5-8: PSS/E GGOV1 turbine and governor

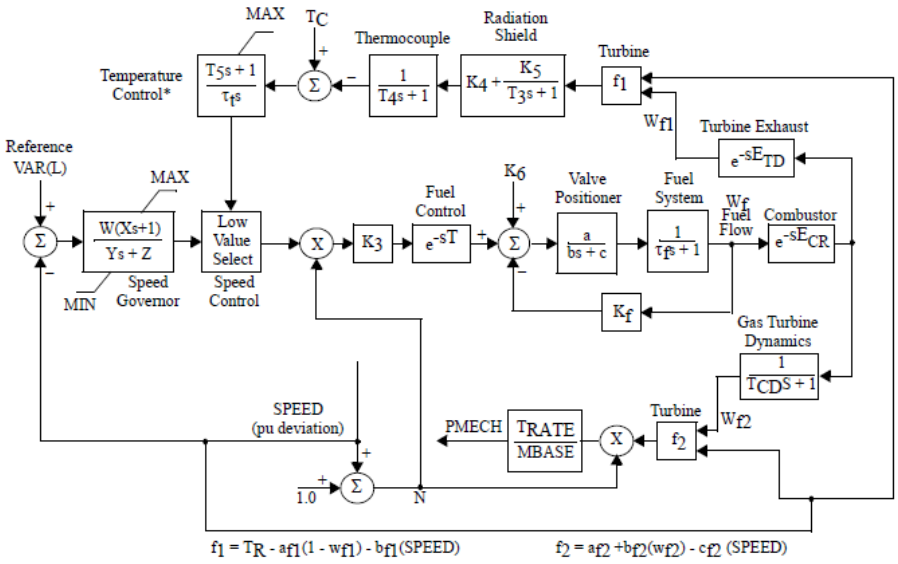

*Temperature control output is set to output of speed governor when temperature control input changes from positive to negative.

Figure 5-9: PSS/E GAST2A turbine and governor

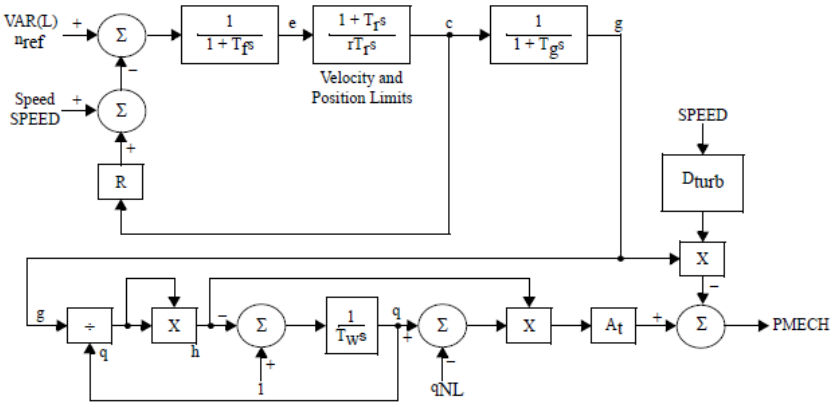

Figure 5-10: PSS/E HYGOV turbine and governor

5.1.2. Dynamic model of the system

The dynamic model of the system is described by a dynamic data file. The dynamic data file is a text file (written according PSS/E rules in FORTRAN free format) that contains the model data of each generating unit.

Whenever detailed models are not available for all generating units for example due to confidentiality reasons, standardized generating unit technologies are used. For each of the major generating unit technologies (nuclear, thermal, gas, hydro, wind, solar thermal and solar photovoltaic) an existing plant is chosen as a standardized reference plant. The concept of reference plant arose from nuclear power generation, where new reactors need to be built according to an existing reference plant. Unless detailed models are available, a reference plant is assigned to each generating unit according to its technology (e.g., thermal or gas power plant). Each reference plant in turn is represented by using typical models of synchronous generator components.

This approach is also meaningful when including transient stability analysis to long-term planning studies. At the planning stage, dynamic parameters of the models of the power system components in general and of generating units and HVDC links in particular are not known yet. Using a reference component (e.g., a reference plant as for generating units) of similar technology and size is a good starting point, making use of the available information most effectively.

5.1.1. Critical clearing time calculation

Figure 5-11 provides an overview for the calculation of the critical clearing time of a fault. Transient stability analyses not only need the steady-state model of the network provided by an AC load flow, but also the dynamic model of generators and other dynamic devices.

For a given fault, the fault is applied for a certain duration and subsequently removed. The dynamic response of the power system to the fault and particularly, the responses of generators in terms of relative angels are simulated. If one relative angle is larger than the critical angle, the system is deemed unstable and the previously applied duration is the critical clearing time. Otherwise, the process is repeated until a critical clearing time is found.

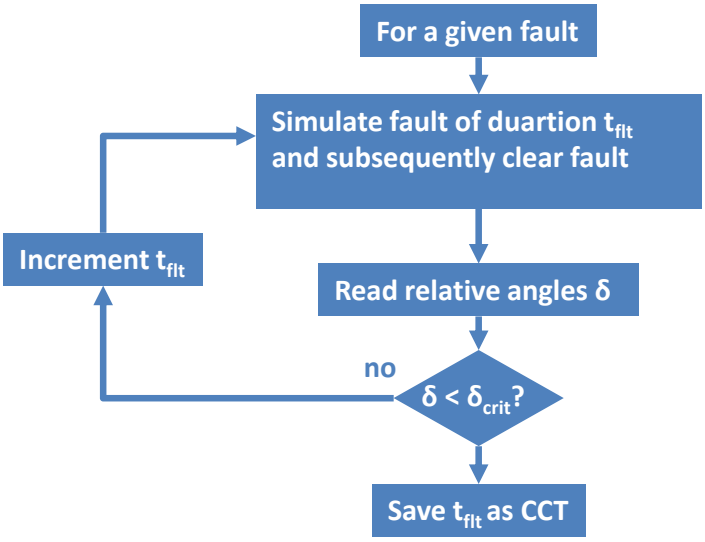

Figure 5-11: Overview of the critical clearing time calculation

5.2. Reduced size illustrative examples

The proposed approach to build a dynamic model is tested firstly on small scale systems obtained from a large scale one. Table 5.I describes the peak load scenario of a large scale test system that corresponds to a model of the French, Spanish and Portuguese power system.

Table 5.I. Peak load scenario of a large scale test system

		GEN	SHUNT	LINES	DEMAND	LOSSES	EXPORT
Spain	P [MW]	83537.1	0	0	55627.9	797.9	27111.2
	Q [MVAr]	-21349.9	2559.4	43734.8	26941.8	6839.1	-8836.9
France	P [MW]	115824.1	0	0	103202.9	1153.7	11467.4
	Q [MVAr]	13673.7	-18950.1	39469.6	49983.5	11001.9	-26792.1
Portugal	P [MW]	13931.1	0	0	11643.3	214.5	2073.3
	Q [MVAr]	-2946.0	441.9	12502.4	5639.1	1446.6	2912.6

5.2.1. Reduced size models

Reduced sized models are obtained from a large model of the French-Spanish-Portuguese power system. Clusters have been obtained using geographical distance. Physical tie-lines among clusters are kept.

Figure 5-12 shows the 24-cluster model. Figure 5-13 provides the cumulative distribution of tie line power flow error. Cumulative distribution of tie lines power flow error. Tie lines are lines connecting different clusters. The tie line power flow error is defined as the difference between the tie line power flow in case of the detailed model and the tie line power flow in case of the reduced model.

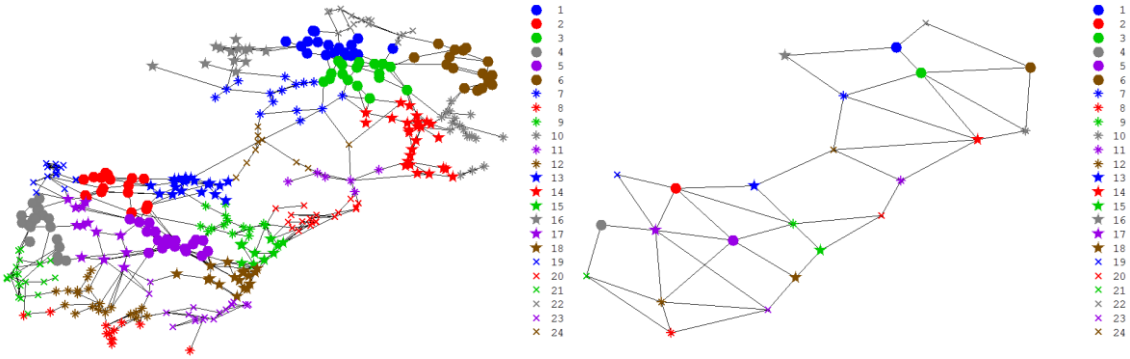

Figure 5-12: 24 cluster model

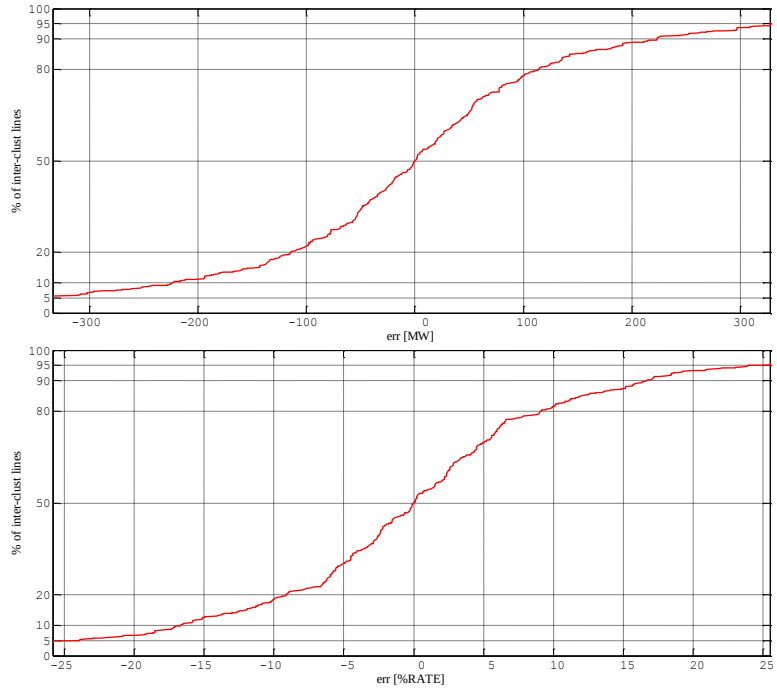

Figure 5-13: Power flow error in the 24-cluster model

5.2.2. Transient stability of the 24-cluster model

Figure 5-14 contains the critical clearing times of the 24-cluster model. The lowest critical clearing time is 0.24 s which is reached in case of a fault at cluster 20. The critical clearing times are in accordance with the most demanding ENTSO-e fault ride through requirement.

Figure 5-15 shows the responses in terms of relative angle of one generator per cluster (including the critically stable one) in case of the critically stable fault at cluster 20. Figure 5-16 displays the generator responses in case of the critically unstable fault at cluster 20. Clearly, a generator looses synchronism during the first power swing.

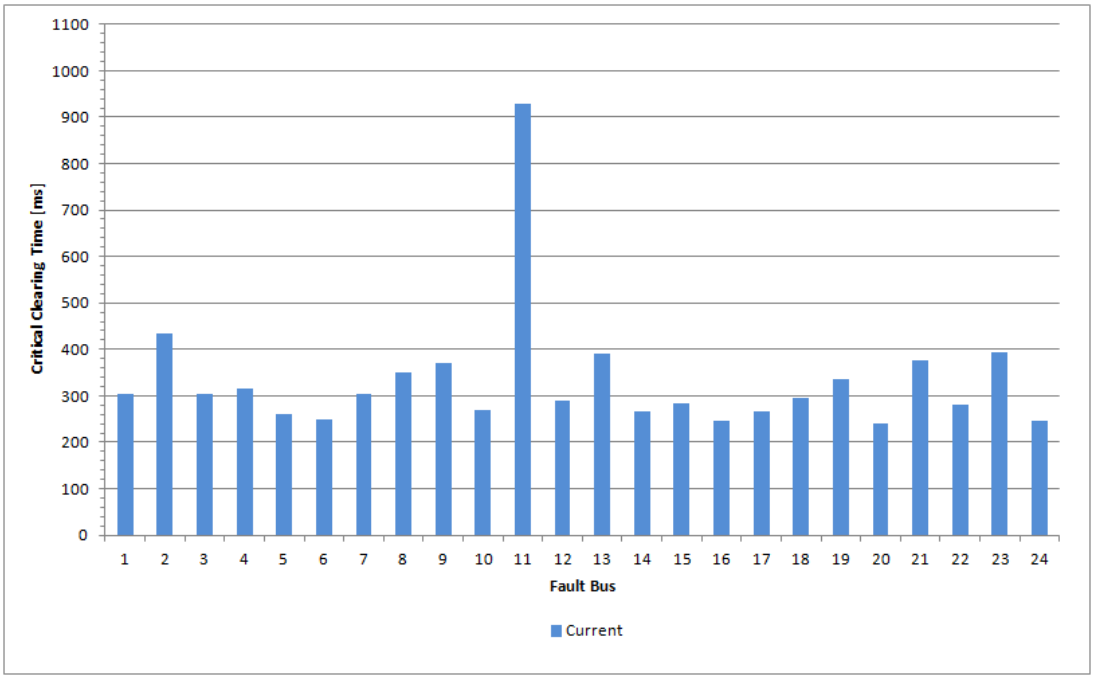

Figure 5-14: Critical clearing times of the 24-cluster model

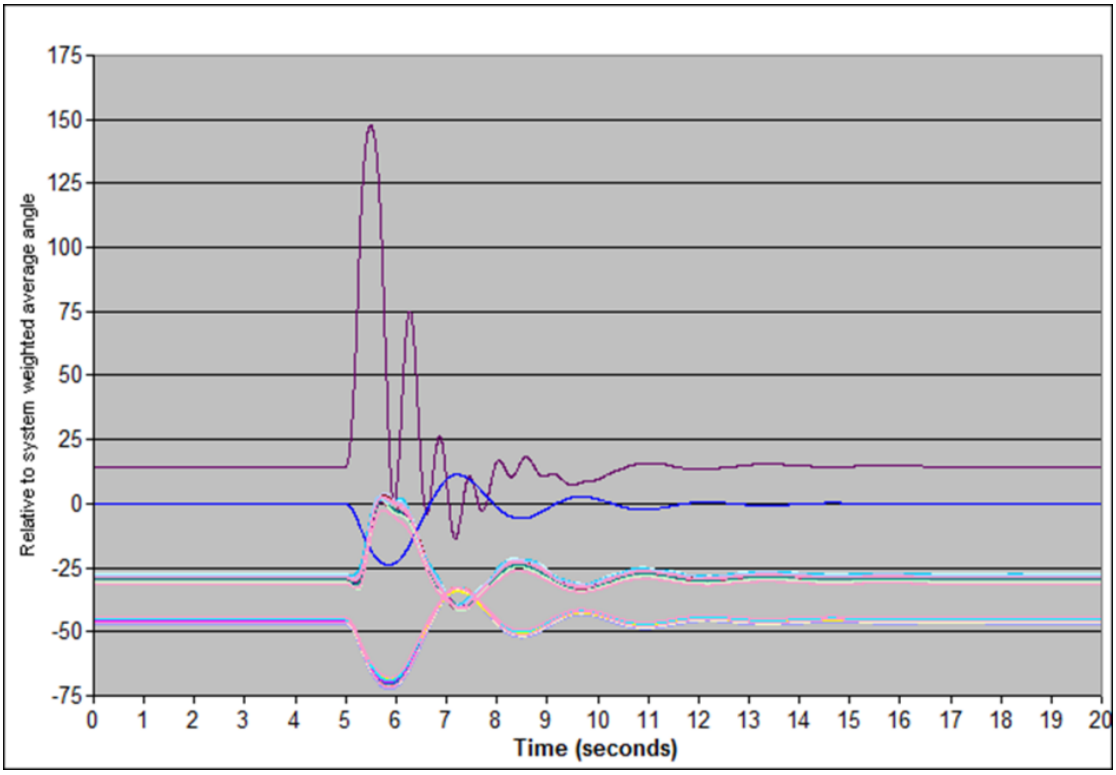

Figure 5-15: 24-cluster model: generator response in case of the critically stable fault at cluster 20

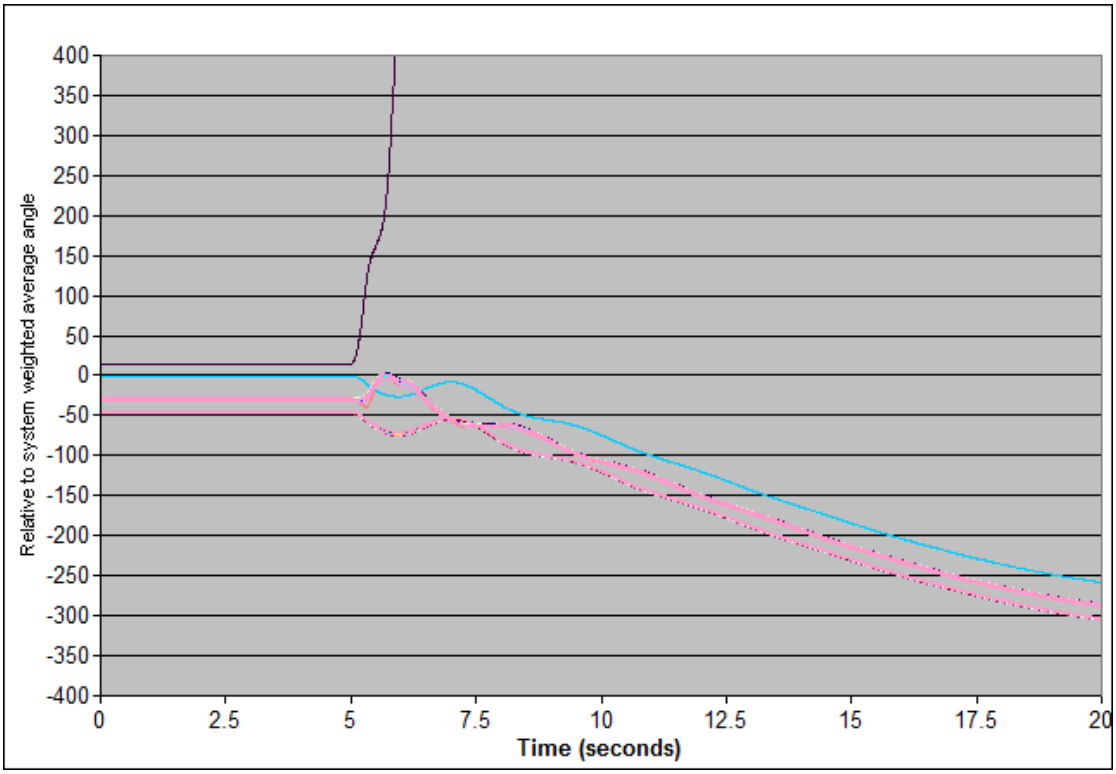

Figure 5-16: 24-cluster model: generator response in case of the critically unstable fault at cluster 20

5.2.3. Transient stability of the 24-cluster model with a moderate increase in export power from Spain to France

The current 24-cluster model has been modified to accommodate an additional 4000 MW of wind power generation. The export from Spain to France increases from 1000 MW to 2000 MW in this case.

Figure 5-14 shows and compares the critical clearing times of the 24-cluster model with current and a moderately increased export. The lowest critical clearing time is still 0.24 s which is reached in case of a fault at cluster 20. Some critical clearing times clearly decreased due to the increase in wind power generation and in exported power, whereas others increased. The critical clearing times are still in accordance with the most demanding ENTSO-e fault ride through requirement.

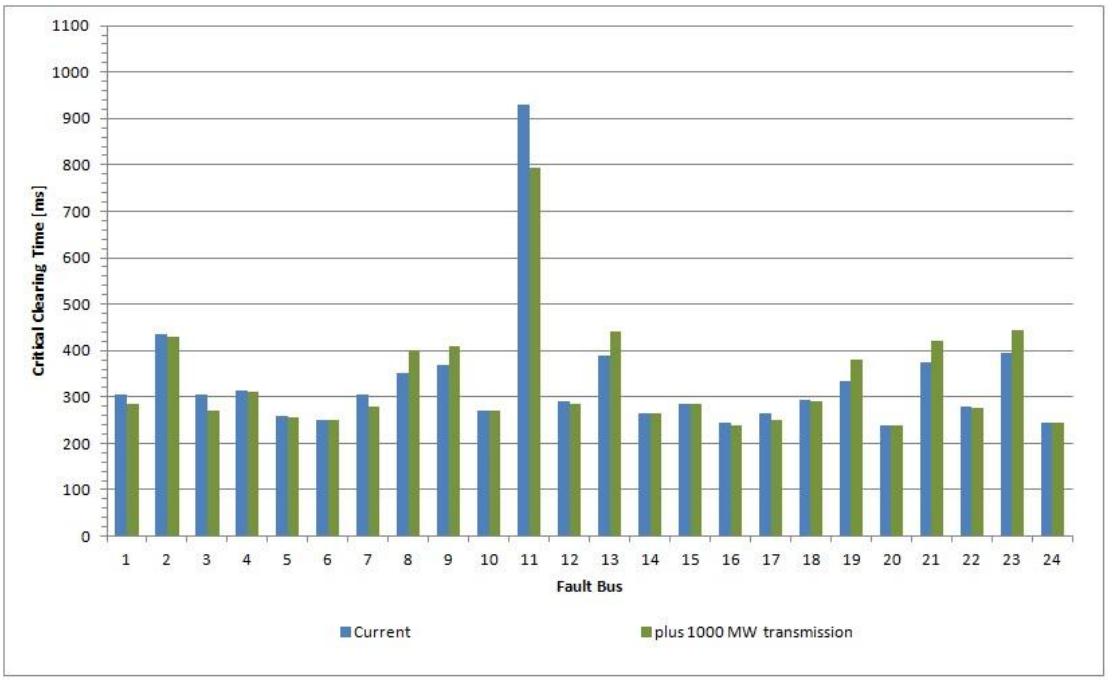

Figure 5-17: Comparison of the critical clearing times of the 24-cluster model with current and a moderately increased export

5.2.4. Transient stability of the 24-cluster model with a large increase in export power from Spain to France

The current 24-cluster model has been modified to accommodate an additional 4000 MW of wind power generation. The export from Spain to France increases from 1000 MW to 4000 MW in this case.

Figure 5-18 shows and compares the critical clearing times of the 24-cluster model with current and a largely increased export. The lowest critical clearing time is now 0.035s which is reached in case of a fault at cluster 15. Critical clearing times are clearly below the most demanding ENTSO-e fault ride through requirement.

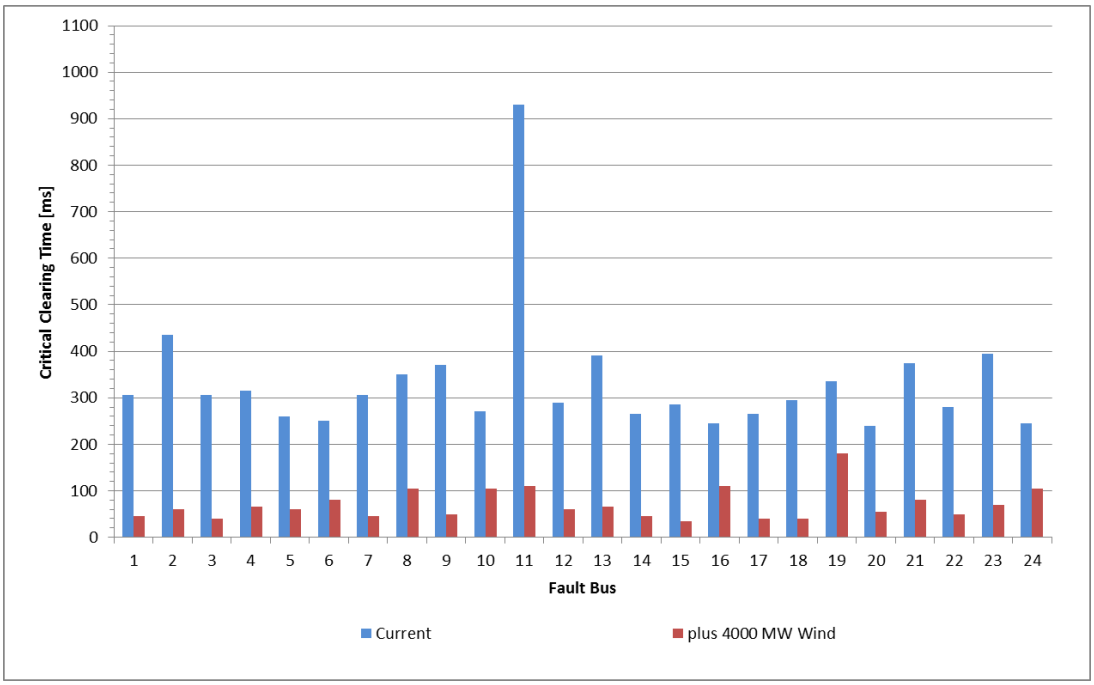

Figure 5-18: Comparison of the critical clearing times of the 24-cluster model with current and a moderately increased export

Figure 5-19 shows the responses in terms of relative angle of one generator per cluster (including the critically stable one) in case of the critically stable fault at cluster 5. Figure 5-20 displays the generator responses in case of the critically unstable fault at cluster 5. Clearly, a generator looses synchronism during a subsequent power swing.

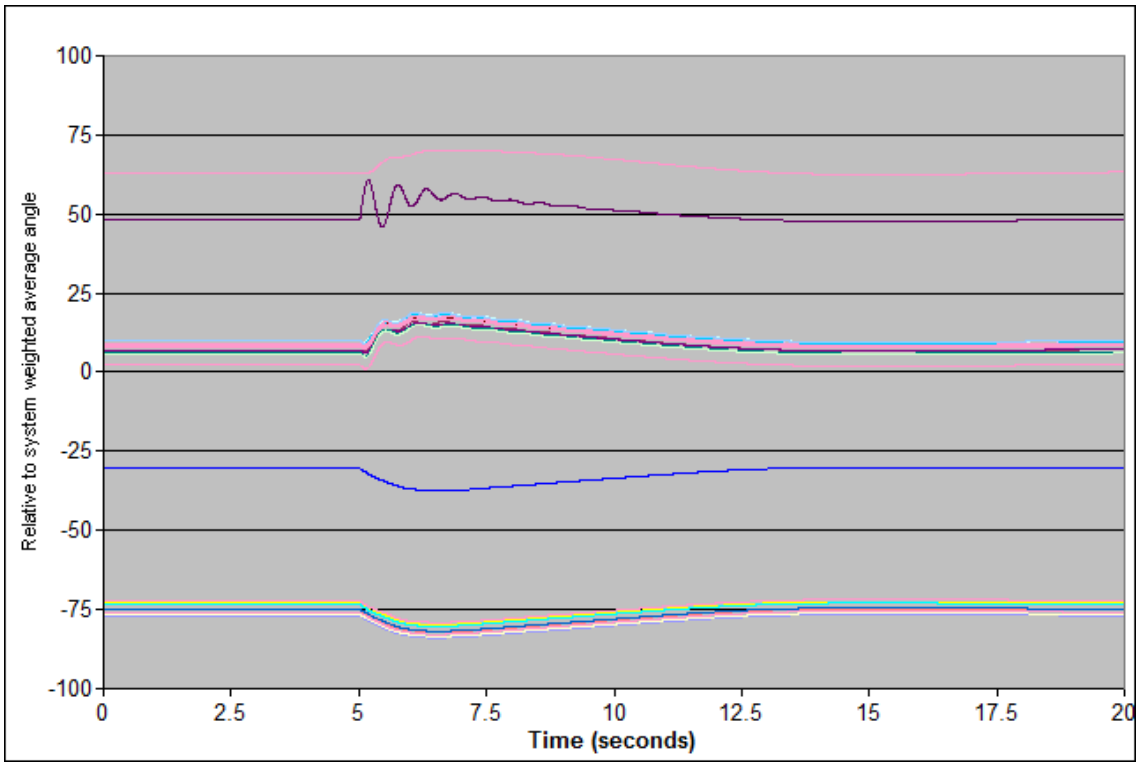

Figure 5-19: 24-cluster model: generator response in case of the critically stable fault at cluster 5

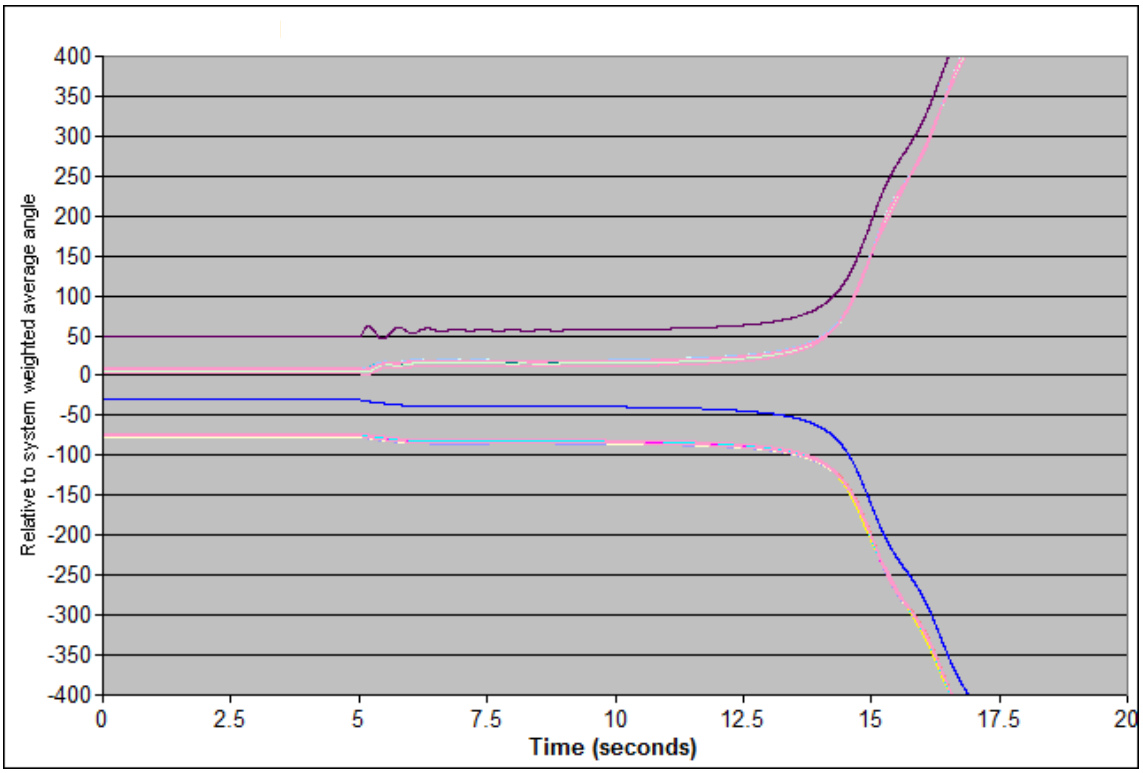

Figure 5-20: 24-cluster model: generator response in case of the critically unstable fault at cluster 5

5.2.5. Transient stability of the 24-cluster model with a large increase in export power from Spain to France with VSC-HVDC links

The current 24-cluster model has been modified to accommodate an additional 4000 MW of wind power generation and by including two VSC-HVDC links. The export from Spain to France increases from 1000 MW to 4000 MW, where 2000 MW flow through the HVDC links. Figure 5-21 shows the modified 24-cluster model.

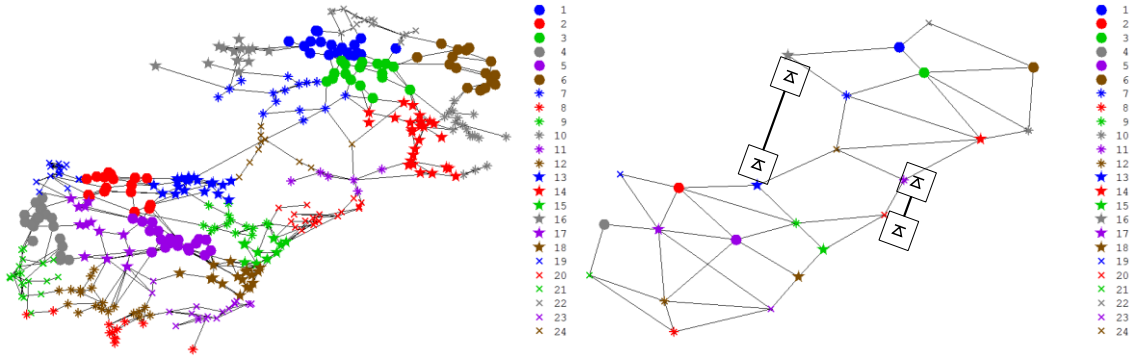

Figure 5-21: 24 cluster model with two VSC-HVDC links

Figure 5-22 shows and compares the critical clearing times with the current and a largely increased power export to France with two HVDC links in the latter case. By comparing Figure 5-22 and Figure 5-18, it can be seen that the HVDC links increase the critical clearing times and bring them back to values prior to the increase of power export.

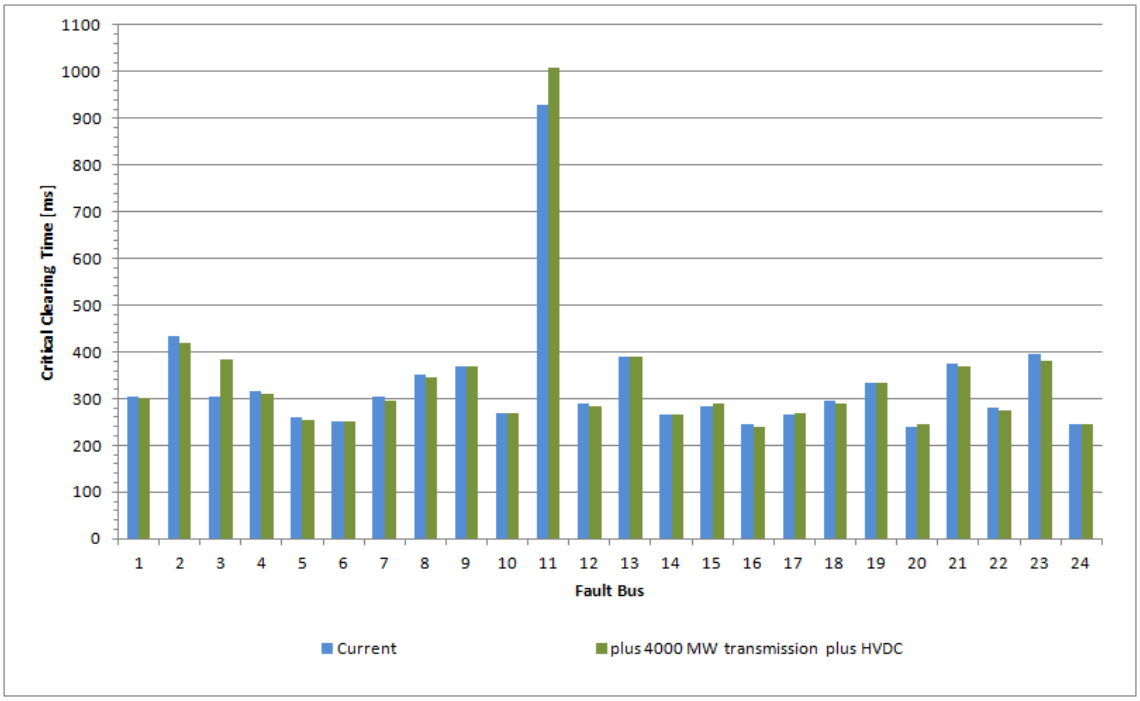

Figure 5-22: Comparison of the critical clearing times of the 24-cluster model with current and a largely increased export with two HVDC links.

Figure 5-23 shows and compares the critical clearing times for the case of a largely increased export with two HVDC links but considering the limited fault ride through capability of the converters. In other words, for faults at or close to the converter terminals, the converter trips after 250 ms. The limited fault ride through capability only affects critical clearing times for faults at buses 7, 11, and 13, where the HVDC links are connected to (the impact of fault at bus 9 is negligible).

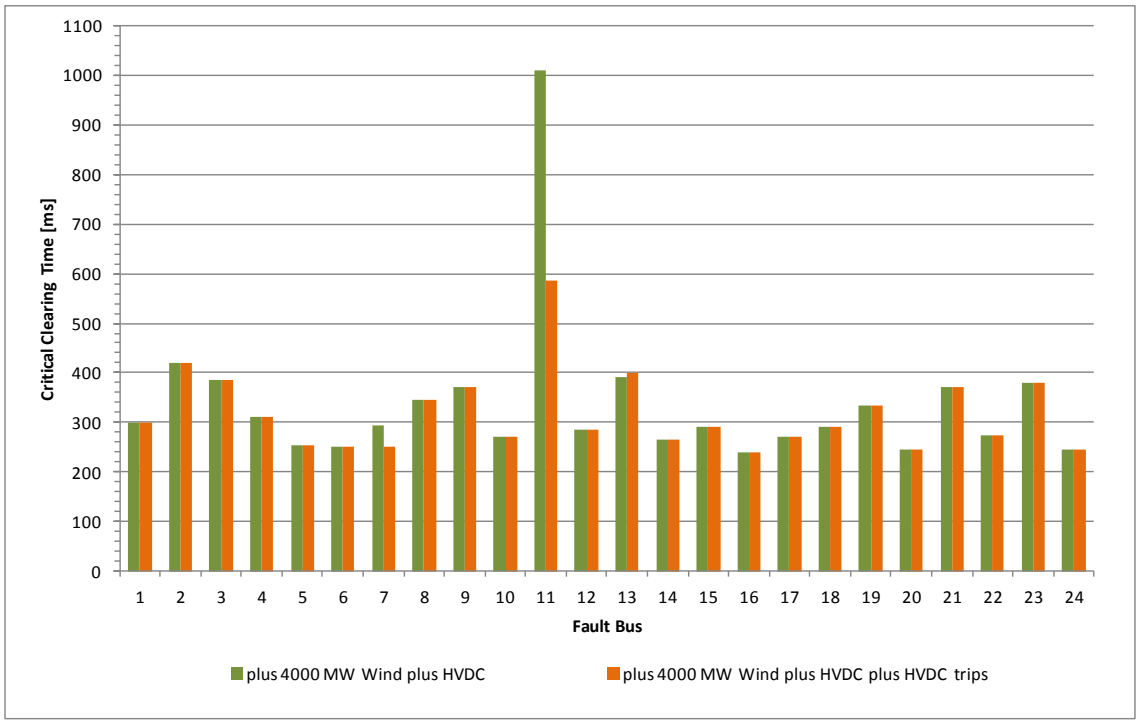

Figure 5-23: Comparison of the critical clearing times of the 24-cluster model with two HVDC links with and without contemplating HVDC tripping.

A possible way to mitigate the impact of low voltage HVDC tripping is redistribute the lost power flow on the remaining HVDC link. A centralized control scheme would be necessary, detecting the HVDC tripping and sending the new power set point to the intact HVDC link. Figure 5-24 shows the critical clearing times considering HVDC tripping and redistribution of active power flow. In fact, the power flow through the remaining link has been increased by about 1000 MW (each pole has been modelled as a proper link). Figure 5-25 shows the responses of the two HVDC links in terms of active power at their terminals.

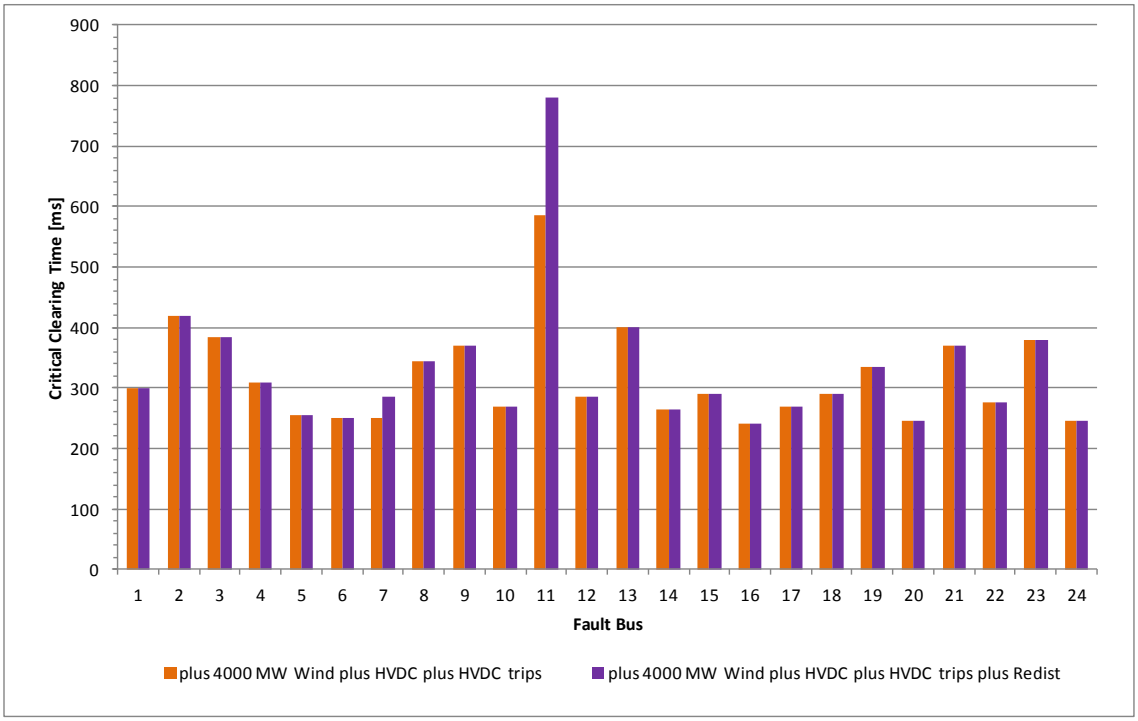

Figure 5-24: Comparison of the critical clearing times of the 24-cluster model with two HVDC links contemplating HVDC tripping with and without controlling active power of the remaining HVDC link

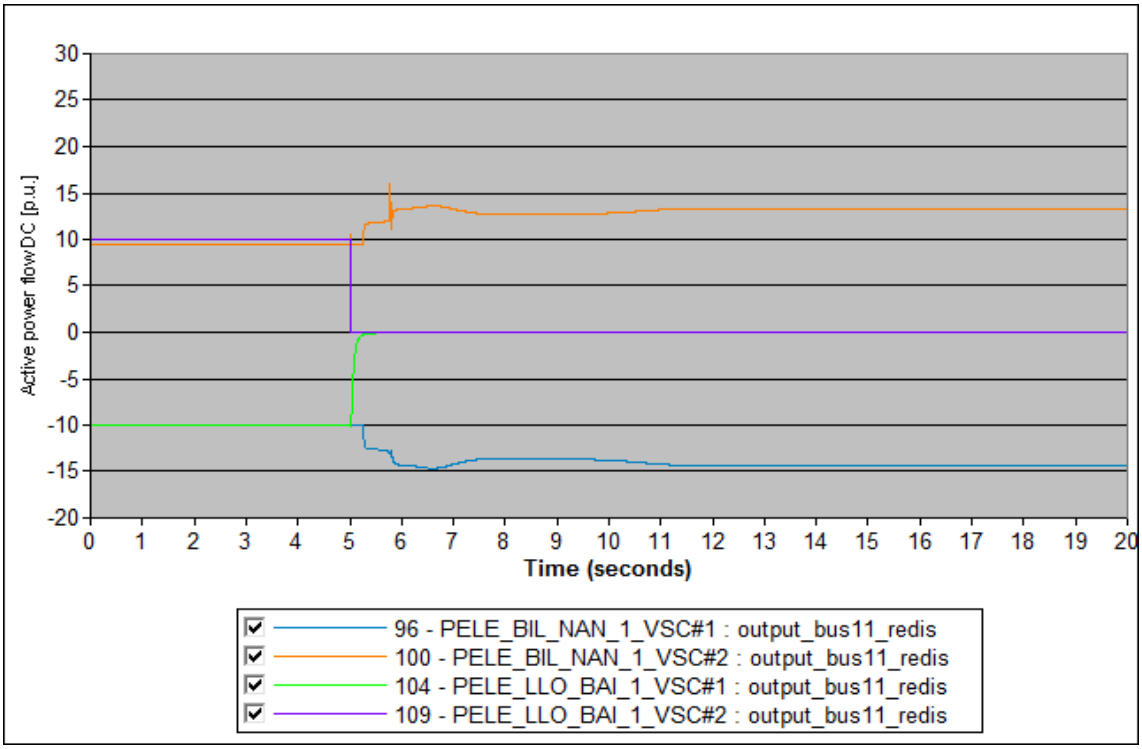

Figure 5-25: Responses in terms of active power of the two HVDC links

Finally, transient stability and particularly critical clearing times can be further improved by modulating active and reactive power set points of the HVDC links (see Figure 4-16). Figure 5-26 shows and compares the critical clearing times when modulating active or reactive power set points. Critical clearing times improve with regard to the previous cases, but for certain faults active power modulation is more appropriate and for other faults reactive power modulation is more effective.

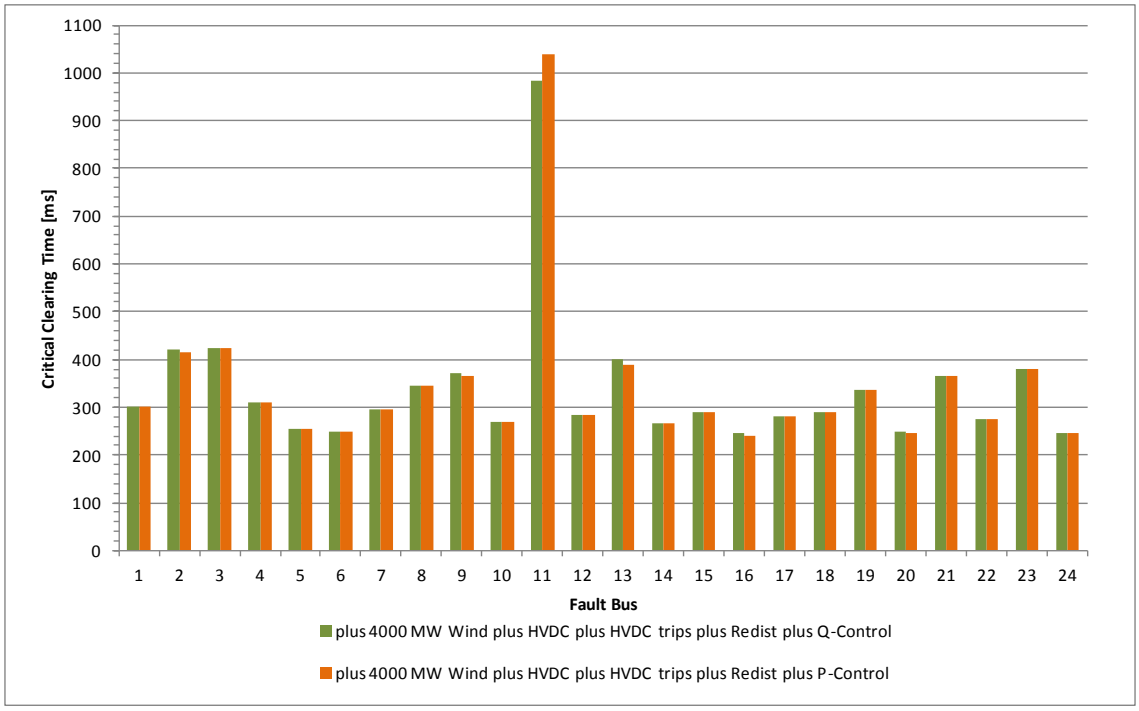

Figure 5-26: Comparison of the critical clearing times of the 24-cluster model with two HVDC links with additional supervisory active and reactive power controls.

5.3. Partial conclusions and discussions

Preliminary results of the procedure to build a dynamic model and to assess transient stability have been shown. Meaningful results have been obtained: the critical clearing times are within the typical range [4].

Wind power generation, power exportation and HVDC transmission influence transient stability. The former two decrease critical clearing times, whereas the latter achieves increasing critical clearing times. In fact, the increase of wind power generation with a moderate increase of power exportation leads to mixed picture of variations of critical clearing times; at some clusters critical clearing times increase, whereas at other clusters they decrease. However, a large increase of power exportation together with an increase of wind power generation leads to very low critical clearing times. Low critical clearing times pose challenges to protection systems. HVDC links are able to increase critical clearing times in this last case. In other words, HVDC link allow for higher power exportation for a given increase in wind power generation without putting at risk system stability. In the light of a 2050 perspective, the likely presence of FACTS devices, the use of synchronous generators as compensators providing additional inertia or inertia emulation by wind farms as in Québec could further improve critical clearing times. However, as long as extremer scenarios in terms of wind power generation and power exportation for the studied Spanish-French system are not available, it is difficult to conclude whether HVDC links are sufficient to stabilize the system or whether these additional options also might be needed.

Finally, the impact of HVDC controls on critical clearing times has been shown. Power flow redistribution among HVDC links in case of HVDC tripping and active and reactive power set point modulation give rise to improved critical clearing times. The improvements are however less spectacular than in the case of the simple two-are four-machine power system. HVDC controls affect thus system stability control performance. The presence of HVDC links requires evaluating the remaining stability controls such as power system stabilizer and a coordinated retuning of the relevant control parameters might be necessary.

6. Conclusions

The following conclusions have been drawn from the work carried out so far:

- A procedure to build an AC load flow model from the DC load flow one has been developed. The procedure dispatches voltage-reactive power control resources to attain AC load flow within an admissible voltage range. However, the main issue of this method was the convergence of the initial load flow which could occur in a planning study and does not occur on actual realized data. If the initial AC load flow does not converge, a new algorithm has been proposed and implemented. It is based on a non-divergent load flow and a sensitivity based algorithm. If a divergent load flow problem occurs, a sequential combination of a non-divergent load flow algorithm and a sensitivity algorithm is used. The performance of the procedure has been tested on actual scenarios of the Spanish and French power systems. The results are very promising.

- The flexibility and robustness of the algorithm to assess voltage stability of large power systems has been shown. The maximum load that generators can serve (or the maximum loadability of the power system) has been determined. The voltage stability of a power system has been measured using the distance to the point of maximum loadability of the power system or point of voltage collapse.

- An investigation on the impact of models and controls of wind generators and HVDC links on the transient stability has been carried out. It has been found that simplified models of power system components should be avoided. Moreover, it has been found that some controls contribute to improve the transient stability of the power system, whereas other controls deteriorate it. Therefore, robustness of grid architectures would rely on appropriate control schemes. Part of the results of this investigation have been summarized in the paper “A fundamental study on the impact of HVDC lines on transient stability of power systems” by L. Sigrist, F. Echavarren, L. Rouco and P. Panciatici that has been accepted for presentation at the IEEE Power Tech 2015.

- Preliminary results of the procedure to build a dynamic model and to assess transient stability have been shown. Meaningful results have been obtained: the critical clearing times are within the typical range. For a given increase of 4000MW in wind power generation in the Spanish-French system, HVDC links allow for higher power exportation to France without putting at risk system stability

7. References

[1] F. Toral, J. Peco, L. Rouco, M.I. Navarrete, A. Mahou, "A Power System Scenarios Builder". Proceedings of the 13th Power Systems Computation Conference, Trondheim, Norway, 28 June - 2 July, 1999, pp. 614-615.

[2] Ministerio de Industria, Comercio y Turismo, "Resolución de 22 de marzo de 2005, de la Secretaría General de Energía, por la que se aprueba el Procedimiento de Operación 13.1-Criterios de Desarrollo de la Red de Transporte- de carácter técnico e instrumental necesario para realizad la adecuada gestión técnica del Sistema Eléctrico", B.O.E. núm. 85, 9 abril 2005, páginas 12351-12358, available at http://ree.es/es/actividades/operacion-del-sistema/procedimientos-de-operacion.

[3] Ministerio de Industria y Energía, "Resolución de 10 de marzo de 2000, de la Secretaría de Estado de Industria y Energía, por la que se aprueba el Procedimiento de Operación 7.4-Servicio complementário de control de tensión de la red de transport", B.O.E. núm. 67, 18 marzo 2000, páginas 11330-11344, available at http://ree.es/es/actividades/operacion-del-sistema/procedimientos-de-operacion.

[4] P. Kundur, "Power System Stability and Control", McGraw - Hill, 1994.

[5] F. Rodríguez-Bobada, P. Ledesma, S. Martínez, L. Coronado, E. Prieto, "Simplified wind generator model for Transmission System Operator planning studies", 7th International Workshop on Large Scale Integration of Wind Power and on Transmission Networks for Offshore Wind Farms, Madrid, Spain, 26 - 27 May, 2008, Paper no. 47.

[6] Siemens Power Technologies International PTI, "Power System Simulator PSS/E Application Guide".

[7] Siemens Power Technologies International PTI, "Power System Simulator PSS/E Operation Manual Manual".

[8] S. Cole, J. Beerten, R. Belmans, "Generalized Dynamic VSC MTDC Model for Power System Stability Studies,", IEEE Transactions on Power Systems, Vol. PWRS-25, No.3, pp. 1655,1662, August 2010.

[9] J. Beerten, S. Cole, R. Belmans, "Modeling of Multi-Terminal VSC HVDC Systems With Distributed DC Voltage Control,", IEEE Transactions on Power Systems, Vol. PWRS-29, No.1, pp.34,42, January 2014.

[10] Eriksson, R., "Coordinated Control of Multiterminal DC Grid Power Injections for Improved Rotor-Angle Stability Based on Lyapunov Theory," Power Delivery, IEEE Transactions on , vol.29, no.4, pp.1789,1797, Aug. 2014.

[11] IEEE Power Engineering Society, "IEEE Guide for Synchronous Generator Modeling Practices in Stability Analyses". IEEE Std. 1110-1991. New York, November 1991.

[12] IEEE, "IEEE Recommended Practice for Excitation System Models forPower System Stability Studies", IEEE Std 421.5-2005.

[13] Working Group on Prime Mover and Energy Supply Models for System Dynamic Performance Studies, "Dynamic Models for Fossil Fueled Steam Units in Power System Studies", IEEE Transactions on Power Systems, Vol. 6, No. 2, May 1991, pp. 753-761.

[14] Working Group on Prime Mover and Energy Supply Models for System Dynamic Performance Studies, "Dynamic models for combined cycle plants in power system studies", IEEE Transactions on Power Systems, Vol. PWRS-9, No. 3, August 1994, pp. 1698 – 1708.

[15] IEEE Working Group on Prime Mover and Energy Supply Models for System Dynamic Performance Studies, “Hydraulic Turbine and Turbine Control Models for System Dynamic Studies”, IEEE Transactions on Power Systems, Vol. PWRS-7, No. 1, February 1992, pp. 167-179.

[16] T. Van Cutsem, C. Vournas, “Voltage Stability of Electric Power systems”, Kluwer Academic Publishers, 1998.

[17] F.M. Echavarren, E. Lobato, L. Rouco, T. Gómez, "Formulation, computation and improvement of steady state security margins in power systems. Part II: Results", International Journal of Electrical Power & Energy Systems. vol. 33, no. 2, pp. 347-358, Feb 2011.

[18] F.M. Echavarren, E. Lobato, L. Rouco, T. Gómez, "Formulation, computation and improvement of steady state security margins in power systems. Part I: Theoretical framework", International Journal of Electrical Power & Energy Systems. vol. 33, no. 2, pp. 340-346, Feb 2011

[19] F.M. Echavarren, E. Lobato, L. Rouco, "Steady-state analysis of the effect of reactive generation limits in voltage stability", Electric Power Systems Research. vol. 79, no. 9, pp. 1292-1299, Sep 2009.

[20] R. Seydel, “From Equilibrium to Chaos. Practical Bifurcation and Stability Analysis”, Elsevier Science Publishing Co., 1988.